AIAA JOURNAL
Vol. 47, No. 6, June 2009

Control of Nonlinear Vibrations of Functionally Graded Plates Using 1-3 Piezoelectric Composite

Satyajit Panda* and M. C. Ray†
Indian Institute of Technology, Kharagpur 721 302, India

DOI: 10.2514/1.38048

Performance of the vertically/obliquely reinforced 1-3 piezoelectric composite material as the constraining layer of the active-constrained-layer damping treatment for controlling geometrically nonlinear vibrations of the functionally graded plates subjected to a temperature field has been investigated. Unlike the existing analyses, the finite element model uses the induced transverse normal stress in the active constraining layer for the active damping of nonlinear vibrations of the overall functionally graded plates. The temperature field is assumed to be uniform over the substrate plate surfaces and varied through the thickness of the host functionally graded plates. The temperature-dependent material properties of the functionally graded substrate plates are assumed to be graded in the thickness direction of the plates according to a power-law distribution, and Poisson's ratio is assumed to be a constant over the domain of the plate. The constrained viscoelastic layer of the active-constrained-layer damping treatment is modeled using the Golla–Hughes–McTavish method. The first-order shear deformation theory and the Green–Lagrange nonlinear strain-displacement relations are used to model the open-loop and closed-loop nonlinear dynamics of the overall functionally graded substrate plates under a thermal environment. The analysis suggests the potential use of the active-constrained-layer damping treatment with its constraining layer made of the vertically reinforced 1-3 piezoelectric composite material for active control of geometrically nonlinear vibrations of functionally graded plates in the absence or presence of the temperature gradient across the thickness of the plates. The analysis also reveals that the active-constrained-layer damping patch is more effective for controlling the nonlinear vibrations of functionally graded plates when it is attached to the softest surface of the functionally graded plates than when it is bonded to the stiffest surface of the plates. The effect of piezoelectric fiber orientation in the active constraining layer on the control authority of the active-constrained-layer damping treatment has also been investigated.

I. Introduction

IN RECENT years, extensive research has been carried out on a new class of composite materials known as functionally graded (FG) materials (FGM). The FGM are nonhomogeneous and attributed by a smooth and continuous variation of material properties, particularly along the thickness direction. In an endeavor to develop the super-heat-resistant materials, Koizumi [1] first proposed the concept of FGM. These materials are microscopically heterogeneous and are typically made from isotropic components, such as metals and ceramics. The traditional laminated composite structures can be tailored to design advanced structures, but the sharp change in properties of each layer at the interface between the two adjacent layers causes large interlaminar shear stresses that eventually may give rise to the initiation of imperfections such as delamination. Such a detrimental effect can be mitigated by grading the properties in a continuous manner across the thickness direction. For example, Teymur et al. [2] carried out the thermomechanical analysis of materials that are functionally graded in two directions and demonstrated that the onset of delamination could be prevented by tailoring the microstructures of the composite plies. Thus, the use of FGM may become an important issue for developing advanced structures. A great deal of research has already been reported on the exact solutions [3,4], dynamic analysis [5–7], and nonlinear thermoelastic analysis [8–11] of structures made of functionally graded materials during the past few years.

In the quest for developing lightweight high-performing flexible structures with self-controlling and/or self-monitoring capabilities, the piezoelectric materials are extensively used by exploiting its converse and direct piezoelectric effects as distributed actuators or sensors that are either surface-mounted or embedded in the host structures [12,13]. Considerable interest has also been focused on investigating the performance of the functionally graded plates integrated with the piezoelectric actuators [14–16]. Further research on the efficient active control of the flexible structures using low-control-authority piezoelectric materials led to the development of the active-constrained-layer damping (ACLD) treatment [17]. The ACLD treatment consists of a layer of viscoelastic material constrained between a host structure and an active constraining layer made of piezoelectric material. During the flexural vibration of the host structures, the active constraining layer not only restrains the constrained viscoelastic layer to undergo transverse shear deformations, but also enhances the transverse shear deformations to cause improved damping characteristics of the overall structure over the conventional passive constrained-layer damping treatment. Hence, the ACLD treatment has earned wide acceptability for efficient and reliable control of flexible structures [18–23].

One of the various piezoelectric composites proposed by the researchers to date is the vertically reinforced 1-3 piezoelectric composite [24] and is commercially available (Materials Systems) in the form of laminas. The constructional feature of a lamina made of this 1-3 piezoelectric composite is that the piezoelectric fibers poled along their length are vertically reinforced in the epoxy matrix across the thickness of the lamina. Because the magnitude of the effective piezoelectric coefficient e_{33} of this piezoelectric composite is much larger than that of the effective coefficient e_{31} [24], the induced normal stress in the thickness direction will be larger than the in-plane normal stress, due to the applied electric field across the thickness of the lamina. This induced normal stress in the thickness direction causes transverse normal actuation and can be exploited for flexural deformation or vibration control.

Recently, Ray and Pradhan [25,26] investigated the contribution of the induced transverse normal stress in such 1-3 piezoelectric composite material for active-constrained-layer damping of composite beams and plates. Panda and Ray [27,28] carried out the static

Received 13 April 2008; accepted for publication 24 December 2008.

*Research Scholar, Department of Mechanical Engineering.
†Professor, Department of Mechanical Engineering.

analysis for the geometrically nonlinear deformations of the FG plates integrated with a layer/patch of distributed actuator made of the vertically reinforced 1-3 piezoelectric composite material. To the authors' best knowledge, no work has yet been reported on the performance of the ACLD treatment for active control of geometrically nonlinear transient vibrations of smart FG plates under a thermal environment using the vertically/obliquely reinforced 1-3 piezoelectric composite.

In this paper, the authors intend to investigate the performance of the vertically/obliquely reinforced 1-3 piezoelectric composite as the material of the active constraining layer of the ACLD treatment for controlling the geometrically nonlinear transient vibrations of FG plates in the absence and the presence of a temperature field through the thickness of the host FG plates. Based on the first-order shear deformation theory and the Green–Lagrange nonlinear strain-displacement relations, a three-dimensional finite element model has been developed to model the open-loop and closed-loop nonlinear dynamics of the FG plates integrated with a patch of ACLD treatment. For time-domain analysis, the constrained viscoelastic layer of the ACLD treatment is modeled by the Golla–Hughes–McTavish (GHM) method [29,30]. The effect of the variation of piezoelectric fiber orientation angle in the piezoelectric composite constraining layer on the performance of the ACLD treatment for controlling the nonlinear vibrations of FG substrate plates has also been investigated.

II. Finite Element Modeling

Figure 1 illustrates a simply supported FG substrate plate made of two homogeneous isotropic materials (ceramic and metal). The top surface of this FG plate is integrated with a patch of ACLD treatment. The constraining layer of the ACLD treatment is made of vertically or obliquely reinforced 1-3 piezoelectric composite material. The FG substrate plate is considered to be subjected to the thermal environment, such that its ceramic-rich and metal-rich surfaces are exposed to the constant temperatures T_c and T_m, respectively. The middle plane of the substrate plate is considered as the reference plane, and the planes parallel to the reference plane are assumed to be isothermal planes. The variation of temperature is considered to occur only through the thickness of the host FG plate. The top surface of the FG plate and the ACLD patch are always exposed to the room temperature ($T_0 = 300$ K), and it is assumed that the FG plate is free of thermal stress at room temperature.

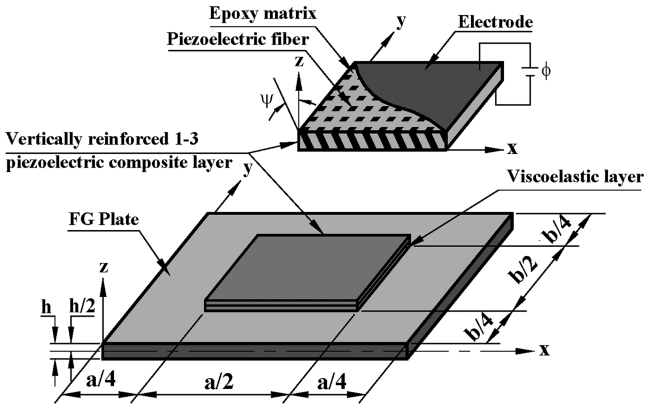

Fig. 1 Schematic diagram of a functionally graded plate integrated with a patch of ACLD treatment.

The origin of the reference coordinate system is located at one corner of the reference plane, such that the lines $x = 0, a$ and $y = 0, b$ represent the boundaries of the FG plate. The thickness of the FG substrate plate, the viscoelastic constrained layer, and the piezoelectric composite constraining layer are denoted by h, h_v, and h_p, respectively. The piezoelectric fibers in the piezoelectric composite layer are coplanar with either the vertical x–z plane or the y–z plane, and their orientation angle with respect to the vertical z axis is denoted by ψ.

Because the thickness of the overall plate is very thin, the first-order shear deformation theory is used to describe the kinematics of axial deformations, as illustrated in Fig. 2, where u_0 and v_0 are the generalized translational displacements of a point on the middle plane of the FG substrate plate along the x and y directions, respectively; θ_x, ϕ_x, and γ_x are the generalized rotations of the normals to the middle planes of the FG substrate plate, the viscoelastic layer, and the piezoelectric composite layer, respectively, about the y axis; and θ_y, ϕ_y, and γ_y are the generalized rotations of these normals about the x axis. According to these kinematics of deformation, the axial displacements u and v at any point in the domain of the overall plate along the x and $y$directions, respectively, can be expressed as

$$u^k(x,y,z,t) = u_0(x,y,t) + \sum_{i=1}^{3} z_i^k(z)\vartheta_x^i(x,y,t)$$

$$v^k(x,y,z,t) = v_0(x,y,t) + \sum_{i=1}^{3} z_i^k(z)\vartheta_y^i(x,y,t)$$

$$z_1^k = (z - \langle z - h/2\rangle), \qquad z_2^k = (\langle z - h/2\rangle - \langle z - h/2 - h_v\rangle)$$

$$z_3^k = \langle z - h/2 - h_v\rangle, \qquad \langle z - h/2\rangle = z - h/2 \quad \text{for } z \geq h/2$$

$$= 0 \quad \text{for } z < h/2$$

$$\langle z - h/2 - h_v\rangle = z - h/2 - h_v \quad \text{for } z \geq (h/2 + h_v)$$

$$= 0 \quad \text{for } z < (h/2 + h_v)$$

$$\vartheta_x^1 = \theta_x, \qquad \vartheta_x^2 = \phi_x, \qquad \vartheta_x^3 = \gamma_x, \qquad \vartheta_y^1 = \theta_y$$

$$\vartheta_y^2 = \phi_y, \qquad \vartheta_y^3 = \gamma_y \tag{1}$$

where the superscript k designates the FG substrate, the viscoelastic layer, and the piezoelectric composite layer according as its value is 1, 2, and 3, respectively; the brackets $\langle\,\rangle$ are used to define the

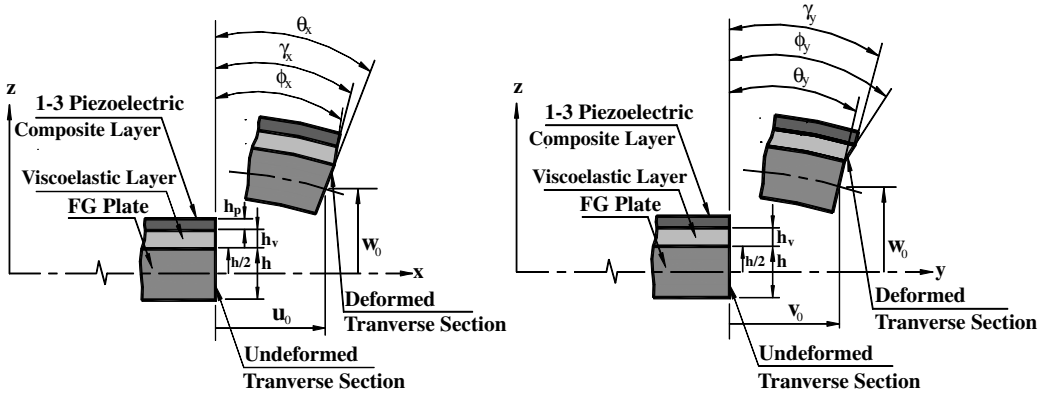

Fig. 2 Deformation of any transverse cross sections of the FG plate integrated with the ACLD treatment which are parallel to y–z and x–z planes.

appropriate singularity functions for satisfying the continuity condition between any two continua. To use the vertical actuation by the active constraining layer as well as the transverse normal strain, the transverse deformation of the overall plate must be considered in deriving the theoretical model. Thus, similar to the in-plane displacements, the transverse displacement at any point of the overall plate can be expressed as

$$w^k(x,y,z,t) = w_0(x,y,t) + \sum_{i=1}^{3} z_i^k(z)\vartheta_z^i(x,y,t)$$
$$\vartheta_z^1 = \theta_z, \qquad \vartheta_z^2 = \phi_z, \qquad \vartheta_z^3 = \gamma_z \tag{2}$$

where w_0 is the transverse displacement at a point on the reference plane, and θ_z, ϕ_z, and γ_z are the gradients of the transverse displacements in the substrate FG plate, the viscoelastic layer, and the piezoelectric composite layer, respectively, with respect to the thickness coordinate z. For the ease of analysis, the generalized displacement variables are separated into translational $\{d_t\}$ and rotational $\{d_r\}$ variables as follows:

$$\{d_t\} = [\,u_0 \quad v_0 \quad w_0\,]^T \quad \text{and}$$
$$\{d_r\} = [\,\theta_x \quad \theta_y \quad \theta_z \quad \phi_x \quad \phi_y \quad \phi_z \quad \gamma_x \quad \gamma_y \quad \gamma_z\,]^T \tag{3}$$

The state of strain at any point of the overall plate is expressed by the following two strain vectors,

$$\{\varepsilon_b\} = \{\,\varepsilon_x \quad \varepsilon_y \quad \varepsilon_{xy} \quad \varepsilon_z\,\}^T \quad \text{and} \quad \{\varepsilon_s\} = \{\,\varepsilon_{xz} \quad \varepsilon_{yz}\,\}^T \tag{4}$$

where ε_x, ε_y, and ε_z are the normal strains along the x, y, and z directions, respectively; ε_{xy} is the in-plane shear strain; and $\varepsilon_{xz}$and ε_{yz} are the transverse shear strains. Similarly, the state of stress at any point of the overall plate is described by the following two stress vectors:

$$\{\sigma_b\} = \{\,\sigma_x \quad \sigma_y \quad \sigma_{xy} \quad \sigma_z\,\}^T \quad \text{and} \quad \{\sigma_s\} = \{\,\sigma_{xz} \quad \sigma_{yz}\,\}^T \tag{5}$$

where σ_x, σ_y, and σ_z are the normal stresses along the x, y, and z directions, respectively; σ_{xy} is the in-plane shear stress; and σ_{xz} and σ_{yz} are the transverse shear stresses. Considering the Green–Lagrange nonlinear strain-displacement relations for small strains and moderate rotations [31], the strain vectors given by Eq. (4) for the kth layer can be expressed as

$$\{\varepsilon_b^k\} = \{\,\tfrac{\partial u^k}{\partial x} + \tfrac{1}{2}(\tfrac{\partial w^k}{\partial x})^2 \quad \tfrac{\partial v^k}{\partial z} + \tfrac{1}{2}(\tfrac{\partial w^k}{\partial y})^2 \quad \tfrac{\partial u^k}{\partial y} + \tfrac{\partial v^k}{\partial x} + \tfrac{\partial w^k}{\partial x}\tfrac{\partial w^k}{\partial y} \quad \tfrac{\partial w^k}{\partial z}\,\}^T$$
$$\{\varepsilon_s^k\} = \{\,\tfrac{\partial u^k}{\partial z} + \tfrac{\partial w^k}{\partial x} \quad \tfrac{\partial v^k}{\partial z} + \tfrac{\partial w^k}{\partial y}\,\}^T \tag{6}$$

Substituting the displacement field given by Eqs. (1) and (2) into Eq. (6), the strain vectors and their first variations in terms of the generalized displacement variables can be expressed as

$$\{\varepsilon_b^k\} = \sum_{i=1}^{2}([Z_i^k][L_i] + [Z_{ni}^k][R_{ni}][L_{ni}])\{d_i\}$$
$$\{\varepsilon_s^k\} = \sum_{i=3}^{4}[Z_i^k][L_i]\{d_i\}$$
$$\{\delta\varepsilon_b^k\} = \sum_{i=5}^{6}([Z_i^k][L_i] + [Z_{ni}^k][R_{ni}][L_{ni}])\{\delta d_i\}$$
$$\{\delta\varepsilon_s^k\} = \sum_{i=7}^{8}[Z_i^k][L_i]\{\delta d_i\} \tag{7}$$

where δ is an operator for first variation. The generalized displacements $\{d_i\}$ and the operator matrices $[L_i]$ and $[L_{ni}]$ (for $i = 1, 2, \ldots, 8$) in the preceding equation are as follows:

$$[L_1] = \begin{bmatrix} \partial/\partial x & 0 & 0 \\ 0 & \partial/\partial y & 0 \\ \partial/\partial y & \partial/\partial x & 0 \\ 0 & 0 & 0 \end{bmatrix}, \qquad [L_2] = \begin{bmatrix} [{}_sL_2] & [0] & [0] \\ [0] & [{}_sL_2] & [0] \\ [0] & [0] & [{}_sL_2] \end{bmatrix}$$
$$[{}_sL_2] = \begin{bmatrix} \partial/\partial x & 0 & 0 \\ 0 & \partial/\partial y & 0 \\ \partial/\partial y & \partial/\partial x & 0 \\ 0 & 0 & 1 \end{bmatrix}, \qquad [L_{n1}] = \begin{bmatrix} 0 & 0 & \partial/\partial x \\ 0 & 0 & \partial/\partial y \end{bmatrix}$$
$$[L_{n2}] = \begin{bmatrix} [L_{n1}] & [0] & [0] \\ [0] & [L_{n1}] & [0] \\ [0] & [0] & [L_{n1}] \end{bmatrix}$$
$$[L_4] = \begin{bmatrix} [{}_sL_4] & [0] & [0] \\ [0] & [{}_sL_4] & [0] \\ [0] & [0] & [{}_sL_4] \end{bmatrix}, \qquad [{}_sL_4] = \begin{bmatrix} 1 & 0 & 0 \\ 0 & 1 & 0 \\ 0 & 0 & \partial/\partial y \\ 0 & 0 & \partial/\partial x \end{bmatrix}$$
$$[L_3] = [L_{n1}], \qquad [L_5] = [L_1], \qquad [L_6] = [L_2], \qquad [L_7] = [L_3]$$
$$[L_8] = [L_4], \qquad [L_{n5}] = [L_{n1}], \qquad [L_{n6}] = [L_{n2}]$$
$$\{d_1\} = \{d_3\} = \{d_5\} = \{d_7\} = \{d_t\}$$
$$\{d_2\} = \{d_4\} = \{d_6\} = \{d_8\} = \{d_r\} \tag{8}$$

The transformation matrices $[Z_i^k]$ and $[Z_{ni}^k]$ and the matrices $[R_{ni}]$ appearing in Eq. (7) are also presented in the Appendix. According to a simple power law, the effective properties of a functionally graded solid composed of two constituent materials (ceramic and metal) can be expressed as

$$P(z) = (P_c - P_m)\{0.5 + (-1)^\lambda z/h\}^r + P_m \tag{9}$$

where P_c and P_m are the properties of ceramic and metal, respectively; r is the power-law exponent ($0 \le r \le \infty$); and λ is a positive integer. When λ is even, the bottom surface of the FG plate is metallic (softest) and the top surface of the plate is ceramic (stiffest), and the reverse holds for odd values of λ. Thus, the top surface of the FG plate can be modeled as the softest surface or the stiffest surface, according to whether λ equals 1 or 2, respectively. Using Eq. (9), the material properties such as Young's modulus $E(z)$, Poisson's ratio $\nu(z)$, the coefficient of thermal expansion $\alpha(z)$, the thermal conductivity $\kappa(z)$, etc., of the FG substrate plate can be determined, which are the functions of the thickness z coordinate. The constitutive relations for the material of the elastic FG plate can be written as [15]

$$\{\sigma_b^k\} = [\bar{C}_{bb}^k](\{\varepsilon_b^k\} - \{\alpha^k\}\Delta T) \quad \text{and} \quad \{\sigma_s^k\} = [\bar{C}_{ss}^k]\{\varepsilon_s^k\} \quad \text{for } k = 1 \tag{10}$$

where

$$[\bar{C}_{bb}^k] = \frac{E(z)}{(1+\nu(z))(1-2\nu(z))}\begin{bmatrix} 1-\nu(z) & \nu(z) & 0 & \nu(z) \\ \nu(z) & 1-\nu(z) & 0 & \nu(z) \\ 0 & 0 & 1/2-\nu(z) & 0 \\ \nu(z) & \nu(z) & 0 & 1-\nu(z) \end{bmatrix}$$
$$[\bar{C}_{ss}^k] = \frac{E(z)}{(1+\nu(z))(1-2\nu(z))}\begin{bmatrix} 1/2-\nu(z) & 0 \\ 0 & 1/2-\nu(z) \end{bmatrix}$$
$$\{\alpha^k\} = [\alpha_x(z) \;\; \alpha_y(z) \;\; 0 \;\; \alpha_z(z)]^T$$
$$\Delta T = T(z) - T_0 \;\text{ for } k = 1 \tag{11}$$

wherein $\alpha_x(z)$, $\alpha_y(z)$, and $\alpha_z(z)$ are the coefficients of thermal expansion in the x, y, and z directions, respectively, and $T(z)$ is the

temperature at any point in the substrate FG plate. The temperature distribution $T(z)$ across the thickness of the FG substrate plate can be determined from the solution of the following one-dimensional steady-state heat conduction equations (8–10):

$$-\frac{d}{dz}\left(\kappa(z)\frac{dT}{dz}\right)=0 \tag{12}$$

where $\kappa(z)$ is the thermal conductivity of the isotropic FG substrate plate. The solution of Eq. (12) is readily available [10,15], satisfying $T=T_c$ at a ceramic-rich surface ($z=-h/2$ or $h/2$ for $\lambda=1$ or 2) and $T=T_m$ at a metal-rich surface ($z=h/2$ or $-h/2$ for $\lambda=1$ or 2). The constitutive relations for the 1-3 vertically reinforced piezoelectric composite material in the ambient temperature can be written as

$$\begin{aligned}
&\{\sigma_b^k\}=[\bar{C}_{bb}^k]\{\varepsilon_b^k\}+[\bar{C}_{bs}^k]\{\varepsilon_s^k\}-[\bar{e}_s]\{\bar{E}\} \quad \text{and}\\
&\{\sigma_s^k\}=[\bar{C}_{sb}^k]\{\varepsilon_b^k\}+[\bar{C}_{ss}^k]\{\varepsilon_s^k\}-[\bar{e}_s]\{\bar{E}\}\\
&\{D\}=[\bar{e}_b]^T\{\varepsilon_b^k\}+[\bar{e}_s]^T\{\varepsilon_s^k\}+[\bar{\in}]\{\bar{E}\} \quad \text{for } k=3
\end{aligned} \tag{13}$$

Note that because the ACLD treatment is under operation at the ambient temperature, the constitutive relations for the viscoelastic and the piezoelectric layers are independent of the temperature field. In Eq. (13), the transformed elastic coefficient matrices $[\bar{C}_{bb}^k]$, $[\bar{C}_{bs}^k]$, $[\bar{C}_{sb}^k]$, and $[\bar{C}_{ss}^k]$; the transformed piezoelectric coefficient matrices $[\bar{e}_b]$ and $[\bar{e}_s]$; and the matrix of transformed dielectric constants $[\bar{\in}]$, referred to as the user coordinate system, are given by

$$[\bar{C}_{bb}^k]=\begin{bmatrix}\bar{C}_{11}^k & \bar{C}_{12}^k & \bar{C}_{16}^k & \bar{C}_{13}^k\\ \bar{C}_{12}^k & \bar{C}_{22}^k & \bar{C}_{26}^k & \bar{C}_{23}^k\\ \bar{C}_{16}^k & \bar{C}_{26}^k & \bar{C}_{66}^k & \bar{C}_{36}^k\\ \bar{C}_{13}^k & \bar{C}_{23}^k & \bar{C}_{36}^k & \bar{C}_{33}^k\end{bmatrix},\qquad [\bar{C}_{bs}^k]=\begin{bmatrix}\bar{C}_{14}^k & \bar{C}_{15}^k\\ \bar{C}_{24}^k & \bar{C}_{25}^k\\ \bar{C}_{46}^k & \bar{C}_{56}^k\\ \bar{C}_{34}^k & \bar{C}_{35}^k\end{bmatrix}$$

$$[\bar{C}_{ss}^k]=\begin{bmatrix}\bar{C}_{55}^k & \bar{C}_{45}^k\\ \bar{C}_{45}^k & \bar{C}_{44}^k\end{bmatrix},\qquad [\bar{C}_{sb}^k]=[\bar{C}_{bs}^k]^T$$

$$[\bar{e}_b]=\begin{bmatrix}\bar{e}_{11} & \bar{e}_{21} & \bar{e}_{31}\\ \bar{e}_{12} & \bar{e}_{22} & \bar{e}_{32}\\ \bar{e}_{16} & \bar{e}_{26} & \bar{e}_{36}\\ \bar{e}_{13} & \bar{e}_{23} & \bar{e}_{33}\end{bmatrix},\qquad [\bar{e}_s]=\begin{bmatrix}\bar{e}_{14} & \bar{e}_{24} & \bar{e}_{34}\\ \bar{e}_{15} & \bar{e}_{25} & \bar{e}_{35}\end{bmatrix}$$

$$[\bar{\in}]=\begin{bmatrix}\bar{\in}_{11} & \bar{\in}_{12} & \bar{\in}_{13}\\ \bar{\in}_{12} & \bar{\in}_{22} & \bar{\in}_{23}\\ \bar{\in}_{13} & \bar{\in}_{23} & \in_{33}\end{bmatrix} \tag{14}$$

The electric field vector $\{\bar{E}\}$ and the electric displacement vector $\{D\}$ appearing in Eq. (13) are given by

$$\{\bar{E}\}=\{E_x \quad E_y \quad E_z\}^T \quad \text{and} \quad \{D\}=\{D_x \quad D_y \quad D_z\}^T \tag{15}$$

where E_x, E_y, and E_z are the electric fields along the x, y, and z axes, respectively; D_x, D_y, and D_z are the corresponding electric displacements. In the present problem, the electric field is considered to act only along the thickness of the piezoelectric composite constraining layer of the ACLD treatment. Thus, recognizing that $E_z=-V/h_p$ with V being the applied voltage difference across the thickness of the piezoelectric composite layer, the electric field vector, referred to as the reference coordinate system, can be expressed as

$$\{\bar{E}\}=\{0 \quad 0 \quad -1/h_p\}^T V=\{H\}V \tag{16}$$

Using the isothermal stress–strain relation for an isotropic linear viscoelastic material [32], the stress vector $\{\sigma_s^k\}$ ($k=2$) for the viscoelastic damping material layer can be written as

$$\{\sigma_s^k\}=G(t)[I]\{\varepsilon_s^k(0)\}+\int_0^t G(t-\tau)[I]\frac{\partial}{\partial\tau}\{\varepsilon_s^k(\tau)\}\mathrm{d}\tau \quad \text{for } k=2 \tag{17}$$

where $G(t)$ is the material relaxation function, the strain vector $\{\varepsilon_s^k(t)\}$ is restricted to zero for $t\in(-\infty,0)$, and the matrix $[I]$ is a (2×2) unit matrix. It is known that the transverse shear deformations of the viscoelastic layer are attributed to the constrained-layer damping of the host structure. The extensional stiffness of the viscoelastic constrained layer is very small as compared with the FG substrate plate and the piezoelectric composite constraining layer. Thus, the extensional counterpart of the strain energy for the viscoelastic layer may be neglected in estimation of the total potential energy of the overall plate. The first variation of the total potential energy T_P and the kinetic energy T_K of the FG substrate plate integrated with a patch of ACLD treatment can be written as [33]

$$\begin{aligned}
\delta T_P=&\frac{1}{2}\int_0^a\int_0^b\Bigg[\sum_{\substack{k=1\\k\neq 2}}^{3}\int_{h_k}^{h_{k+1}}\{\delta\varepsilon_b^k\}^T\{\sigma_b^k\}\mathrm{d}z\\
&+\sum_{k=1}^{3}\int_{h_k}^{h_{k+1}}\{\delta\varepsilon_s^k\}^T\{\sigma_s^k\}\mathrm{d}z-\int_{h_k}^{h_{k+1}}\{\delta\bar{E}\}^T\{D\}|_{k=3}\mathrm{d}z-2p\delta w\Bigg]\mathrm{d}x\mathrm{d}y
\end{aligned} \tag{18}$$

$$\delta T_K=\frac{1}{2}\int_0^a\int_0^b\left[\sum_{k=1}^{3}\int_{h_k}^{h_{k+1}}(\rho^k\{\delta\dot{d}_t\}^T\{\dot{d}_t\})\mathrm{d}z\right]\mathrm{d}x\mathrm{d}y \tag{19}$$

where $p(x,y,t)$ is a uniformly distributed transverse step load and ρ^k is the mass density of the kth layer. Because the overall plate is very thin, the rotary inertia of the overall plate may be neglected, and hence the rotational velocities are not considered to estimate the kinetic energy of the overall plate. The overall plate is discretized by the eight-noded isoparametric quadrilateral element. Thus, the generalized displacement vectors at any point within the element can be written as

$$\{d_t\}=[N_t]\{d_t^e\} \quad \text{and} \quad \{d_r\}=[N_r]\{d_r^e\} \tag{20}$$

where $\{d_t^e\}$ and $\{d_r^e\}$ are the nodal generalized translational and rotational displacement vectors, respectively, and the matrices $[N_t]$ and $[N_r]$ are the shape-function matrices. The nonlinear equations of motion for the FG substrate plates integrated with the ACLD treatment are derived by employing the extended Hamilton's principle for the nonconservative system [34]:

$$\int_{t_1}^{t_2}(\delta T_k-\delta T_p)\mathrm{d}t=0 \tag{21}$$

Substituting Eqs. (18) and (19) into Eq. (21) and then using Eqs. (7), (10), (13), (17), and (20), the nonlinear governing equations of motion for a typical element of the FG substrate plate integrated with the ACLD treatment can be derived as

$$\begin{aligned}
&[M]^e\{\ddot{d}_t^e\}+[K_{tt}]^e\{d_t^e\}+[K_{tr}]^e\{d_r^e\}\\
&\quad+[K_{tt}^v]^e\left(G(t)\{d_t^e(0)\}+\int_0^t\left[G(t-\tau)\frac{\partial}{\partial\tau}\{d_t^e(\tau)\}\right]\mathrm{d}\tau\right)\\
&\quad+[K_{tr}^v]^e\left(G(t)\{d_r^e(0)\}+\int_0^t\left[G(t-\tau)\frac{\partial}{\partial\tau}\{d_r^e(\tau)\}\right]\mathrm{d}\tau\right)\\
&\quad=\{F_{et}\}^eV+\{F_{Tt}\}^e+\{F_m\}^e
\end{aligned} \tag{22}$$

$$\begin{aligned}
&[K_{rt}]^e\{d_t^e\}+[K_{rr}]^e\{d_r^e\}+[K_{rt}^v]^e\Bigg(G(t)\{d_t^e(0)\}\\
&\quad+\int_0^t\left[G(t-\tau)\frac{\partial}{\partial\tau}\{d_t^e(\tau)\}\right]\mathrm{d}\tau\Bigg)\\
&\quad+[K_{rr}^v]^e\left(G(t)\{d_r^e(0)\}+\int_0^t\left[G(t-\tau)\frac{\partial}{\partial\tau}\{d_r^e(\tau)\}\right]\mathrm{d}\tau\right)\\
&\quad=\{F_{er}\}^eV+\{F_{Tr}\}
\end{aligned} \tag{23}$$

wherein the elemental stiffness matrices $[K_{tt}]^e$, $[K_{tr}]^e$, $[K_{rt}]^e$, $[K_{rr}]^e$, $[K^v_{tt}]^e$, $[K^v_{tr}]^e$, $[K^v_{rt}]^e$, and $[K^v_{rr}]^e$; the elemental mass matrix $[M]^e$; the elemental electroelastic coupling vectors $\{F_{et}\}^e$ and $\{F_{er}\}^e$; the thermal load vectors $\{F_{Tt}\}^e$ and $\{F_{Tr}\}^e$; and the mechanical load vector $\{F_m\}^e$ are derived as follows:

$$[K_{tt}]^e = \int_0^{a_e}\int_0^{b_e}([Q^{bb}_{ji}]|_{\substack{j=5\\i=1}} + [Q^{bs}_{ji}]|_{\substack{j=5\\i=3}} + [Q^{sb}_{ji}]|_{\substack{j=7\\i=1}} + [Q^{ss}_{ji}]|_{\substack{j=7\\i=3}})\mathrm{d}x\mathrm{d}y$$

$$[K_{tr}]^e = \int_0^{a_e}\int_0^{b_e}([Q^{bb}_{ji}]|_{\substack{j=5\\i=2}} + [Q^{bs}_{ji}]|_{\substack{j=5\\i=4}} + [Q^{sb}_{ji}]|_{\substack{j=7\\i=2}} + [Q^{ss}_{ji}]|_{\substack{j=7\\i=4}})\mathrm{d}x\mathrm{d}y$$

$$[K_{rt}]^e = \int_0^{a_e}\int_0^{b_e}([Q^{bb}_{ji}]|_{\substack{j=6\\i=1}} + [Q^{bs}_{ji}]|_{\substack{j=6\\i=3}} + [Q^{sb}_{ji}]|_{\substack{j=8\\i=1}} + [Q^{ss}_{ji}]|_{\substack{j=8\\i=3}})\mathrm{d}x\mathrm{d}y$$

$$[K_{rr}]^e = \int_0^{a_e}\int_0^{b_e}([Q^{bb}_{ji}]|_{\substack{j=6\\i=2}} + [Q^{bs}_{ji}]|_{\substack{j=6\\i=4}} + [Q^{sb}_{ji}]|_{\substack{j=8\\i=2}} + [Q^{ss}_{ji}]|_{\substack{j=8\\i=4}})\mathrm{d}x\mathrm{d}y$$

$$([K^v_{tt}]^e, [K^v_{tr}]^e) = \int_0^{a_e}\int_0^{b_e}([Q^{vss}_{ji}]|_{\substack{j=7\\i=3}}, [Q^{vss}_{ji}]|_{\substack{j=7\\i=4}})\mathrm{d}x\mathrm{d}y$$

$$([K^v_{rt}]^e, [K^v_{rr}]^e) = \int_0^{a_e}\int_0^{b_e}([Q^{vss}_{ji}]|_{\substack{j=8\\i=3}}, [Q^{vss}_{ji}]|_{\substack{j=8\\i=4}})\mathrm{d}x\mathrm{d}y$$

$$(\{F_{et}\}^e, \{F_{er}\}^e) = \int_0^{a_e}\int_0^{b_e}(\{G^b_j\}|_{j=5} + \{G^s_j\}|_{j=7}, \{G^b_j\}|_{j=6} + \{G^s_j\}|_{j=8})\mathrm{d}x\mathrm{d}y$$

$$(\{F_{Tt}\}^e, \{F_{Tr}\}^e) = \int_0^{a_e}\int_0^{b_e}(\{P_j\}|_{j=5}, \{P_j\}|_{j=6})\mathrm{d}x\mathrm{d}y$$

$$[M]^e = \int_0^{a_e}\int_0^{b_e}\bar{m}[N_t]^T[N_t]\mathrm{d}x\mathrm{d}y$$

$$\{F_m\}^e = \int_0^{a_e}\int_0^{b_e}[N_t]^T\{f\}\mathrm{d}x\mathrm{d}y$$

$$[Q^{bb}_{ji}] = [B_j]^T([A_{jbi}][B_i] + [A_{jbni}][R_{ni}][B_{ni}]) + [B_{nj}]^T[R_{nj}]^T([A_{jnbi}][B_i] + [A_{jnbni}][R_{ni}][B_{ni}])$$

$$[Q^{bs}_{ji}] = [B_j]^T[A_{jci}][B_i] + [B_{nj}]^T[R_{nj}]^T[A_{jnci}][B_i]$$

$$[Q^{ss}_{ji}] = [B_j]^T[A_{jsi}][B_i], \qquad [Q^{vss}_{ji}] = [B_j]^T[A^v_{jsi}][B_i]$$

$$[Q^{sb}_{ji}] = [B_j]^T([A_{jdi}][B_i] + [A_{jdni}][R_{ni}][B_{ni}])$$

$$\{G^b_j\} = [B_i]^T\{A_{jbe}\} + [B_{nj}]^T[R_{nj}]^T\{A_{jnbe}\}$$

$$\{G^s_j\} = [B_j]^T\{A_{jse}\}$$

$$\{P_j\} = [B_j]^T\{A_{jTt}\} + [B_{nj}]^T[R_{nj}]^T\{A_{jnTt}\} \tag{24}$$

where a_e and b_e are the length and width of a typical element, and the various strain-nodal displacement matrices, rigidity matrices, mass parameter $\bar{m}$, and load vector $\{f\}$ are given by

$$([B_q], [B_{nq}]) = ([L_q], [L_{nq}])[N_t] \quad \text{for } q = 1, 3, 5, 7$$

$$([B_q], [B_{nq}]) = ([L_q], [L_{nq}])[N_r] \quad \text{for } q = 2, 4, 6, 8$$

$$([A_{jbi}], [A_{jci}], [A_{jdi}], [A_{jsi}]) = \sum_{\substack{k=1\\k\neq 2}}^{3}\int_{h_k}^{h_{k+1}}[Z^k_j]^T([\bar{C}^k_{bb}], [\bar{C}^k_{bs}], [\bar{C}^k_{sb}], [\bar{C}^k_{ss}])[Z^k_i]\mathrm{d}z$$

$$([A_{jbni}], [A_{jdni}]) = \sum_{\substack{k=1\\k\neq 2}}^{3}\int_{h_k}^{h_{k+1}}[Z^k_j]^T([\bar{C}^k_{bb}], [\bar{C}^k_{sb}])[Z^k_{ni}]\mathrm{d}z$$

$$[A_{jnbni}] = \sum_{\substack{k=1\\k\neq 2}}^{3}\int_{h_k}^{h_{k+1}}[Z^k_{nj}]^T[\bar{C}^k_{bb}][Z^k_{ni}]\mathrm{d}z$$

$$([A_{jnbi}], [A_{jnci}]) = \sum_{\substack{k=1\\k\neq 2}}^{3}\int_{h_k}^{h_{k+1}}[Z^k_{nj}]^T([\bar{C}^k_{bb}], [\bar{C}^k_{bs}])[Z^k_i]\mathrm{d}z$$

$$\{A_{jse}\} = \int_{h_k}^{h_{k+1}}[Z^k_j]^T[\bar{e}_s]\{H\}|_{k=3}\mathrm{d}z$$

$$(\{A_{jbe}\}, \{A_{jnbe}\}) = \int_{h_k}^{h_{k+1}}([Z^k_j]^T, [Z^k_{nj}]^T)[\bar{e}_b]\{H\}|_{k=3}\mathrm{d}z$$

$$\{f\} = [0 \quad 0 \quad p]^T, \qquad \bar{m} = \sum_{k=1}^{3}\int_{h_k}^{h_{k+1}}\rho^k\mathrm{d}z$$

$$[A^v_{jsi}] = \int_{h_k}^{h_{k+1}}([Z^k_j]^T[I][Z^k_i])|_{k=2}\mathrm{d}z$$

$$(\{A_{jTt}\}, \{A_{jnTt}\}) = \int_{h_k}^{h_{k+1}}([Z^k_j]^T, [Z^k_{nj}]^T)[\bar{C}^k_{bb}]\{\alpha^k\}\Delta T|_{k=1}\mathrm{d}z \tag{25}$$

Note that because the substrate FG plate is isotropic elastic material, the matrices $[\bar{C}^k_{bs}]$ and $[\bar{C}^k_{sb}]$ for $k = 1$ are the null matrices. Also note that in the preceding formulation, the bending and shear counterparts of the stiffness matrices are formulated separately, such that the selective integration scheme can be implemented in a straightforward manner.

In the Laplace domain, the function $s\tilde{G}(s)$ is referred to as the material modulus function [30], with $\tilde{G}(s)$ being the Laplace transform of material relaxation function $G(t)$ of the viscoelastic material. According to the GHM method for modeling the viscoelastic material in the time domain, this material modulus function is represented by a series of minioscillator terms as follows [30]:

$$s\tilde{G}(s) = G^{\infty}\left[1 + \sum_{q=1}^{R}\alpha_q\frac{s^2 + 2\hat{\xi}_q\hat{\omega}_q s}{s^2 + 2\hat{\xi}_q\hat{\omega}_q s + \hat{\omega}_q^2}\right] \tag{26}$$

where G^{∞} corresponds to the equilibrium value of the modulus [i.e., the final value of $G(t)$]. Each minioscillator term is a second-order rational function involving three positive constants: α_q, $\hat{\xi}_q$, and $\hat{\omega}_q$. These constants govern the shape of the modulus function in the complex domain [30]. Now considering a GHM material modulus function with one minioscillator term [30], that is,

$$s\tilde{G}(s) = G^{\infty}\left[1 + \alpha\frac{s^2 + 2\hat{\xi}\,\hat{\omega}\,s}{s^2 + 2\hat{\xi}\,\hat{\omega}\,s + \hat{\omega}^2}\right] \tag{27}$$

the auxiliary dissipation coordinates $\{z_t\}$, $\{z_r\}$ are introduced as follows [30]:

$$\{\tilde{z}_t(s)\} = \frac{\hat{\omega}^2}{s^2 + 2\hat{\xi}\,\hat{\omega}\,s + \hat{\omega}^2}\{\tilde{X}_t(s)\} \quad \text{and}$$
$$\{\tilde{z}_r(s)\} = \frac{\hat{\omega}^2}{s^2 + 2\hat{\xi}\,\hat{\omega}\,s + \hat{\omega}^2}\{\tilde{X}_r(s)\} \tag{28}$$

where $\{\tilde{z}_t(s)\}$ and $\{\tilde{z}_r(s)\}$ are the Laplace transforms of $\{z_t\}$ and $\{z_r\}$, respectively, and $\{\tilde{X}_t(s)\}$ and $\{\tilde{X}_r(s)\}$ are the Laplace transform of the global nodal translational displacement vector $\{X_t\}$ and the global nodal rotational displacement vector $\{X_r\}$, respectively. Taking an inverse Laplace transform of Eq. (28), the time-domain representation of auxiliary dissipation coordinates can be written as

$$\{\ddot{z}_t\} + 2\hat{\omega}\,\hat{\xi}\{\dot{z}_t\} + \hat{\omega}^2\{z_t\} - \hat{\omega}^2\{X_t\} = 0 \tag{29}$$

$$\{\ddot{z}_r\} + 2\hat{\omega}\,\hat{\xi}\{\dot{z}_r\} + \hat{\omega}^2\{z_r\} - \hat{\omega}^2\{X_r\} = 0 \tag{30}$$

In the feedback control strategy, the control voltage supplied to the ACLD patch can be expressed in terms of the velocities of the global nodal degrees of freedom as follows:

$$V = -k_d\dot{w} = -k_d[N]\{\dot{X}_t\} \tag{31}$$

where $k_d$is the velocity feedback control gain, and $[N]$ is a row matrix defining the location of sensing the velocity signal that will be fed back to the patch. After assembling the elemental governing equations of motion (22) and (23) in the global space, the velocity feedback control strategy (31) is invoked for deriving the closed-loop governing equations of motion of the FG plate integrated with the ACLD patch. Making use of Eqs. (27) and (28) in the Laplace transform of the closed-loop governing equations and subsequently taking inverse Laplace transform of the resulting equations, the following global equations of motion are obtained:

$$[M]\{\ddot{X}_t\} + [C_{tt}]\{\dot{X}_t\} + [K^c_{tt}]\{X_t\} + [K^c_{tr}]\{X_r\} + [K^d_{tt}]\{z_t\} + [K^d_{tr}]\{z_r\} = \{F_{Tt}\} + \{F_m\} \tag{32}$$

$$[C_{rt}]\{\dot{X}_t\} + [K^c_{rt}]\{X_t\} + [K^c_{rr}]\{X_r\} + [K^d_{rt}]\{z_t\} + [K^d_{rr}]\{z_r\} = \{F_{Tr}\} \tag{33}$$

where

$$[C_{tt}] = k_d\{F_{et}\}[N], \qquad [C_{rt}] = k_d\{F_{er}\}[N]$$
$$[K^c_{tt}] = [K_{tt}] + [K^v_{tt}]G^\infty(1+\alpha), \qquad [K^d_{tt}] = -[K^v_{tt}]G^\infty\alpha$$
$$[K^c_{tr}] = [K_{tr}] + [K^v_{tr}]G^\infty(1+\alpha), \qquad [K^d_{tr}] = -[K^v_{tr}]G^\infty\alpha$$
$$[K^c_{rt}] = [K_{rt}] + [K^v_{rt}]G^\infty(1+\alpha)$$
$$[K^c_{rr}] = [K_{rr}] + [K^v_{rr}]G^\infty(1+\alpha), \qquad [K^d_{rt}] = -[K^v_{rt}]G^\infty\alpha$$
$$[K^d_{rr}] = -[K^v_{rr}]G^\infty\alpha \tag{34}$$

wherein $[K_{tt}]$, $[K_{tr}]$, $[K_{rt}]$, $[K_{rr}]$, $[K^v_{tt}]$, $[K^v_{tr}]$, $[K^v_{rt}]$, and $[K^v_{rr}]$ are the global stiffness matrices; $[M]$ is the global mass matrix; $\{F_m\}$ is the global nodal mechanical force vector; $\{F_{et}\}$ and $\{F_{er}\}$ are the global electroelastic coupling vectors; and $\{F_{Tt}\}$ and $\{F_{Tr}\}$ are the global nodal thermal load vectors. After imposing the boundary conditions, the global rotational degrees of freedom $\{X_r\}$ can be condensed from Eqs. (29), (30), and (32) to obtain the following final global closed-loop equations of motion in terms of the global nodal translational degrees of freedoms $\{X_t\}$ and the dissipative coordinates $\{z_t\}$ and $\{z_r\}$ as follows:

$$[\bar{M}]\{\ddot{\bar{X}}(t)\} + [\bar{C}]\{\dot{\bar{X}}(t)\} + [\bar{K}]\{\bar{X}(t)\} = \{\bar{F}\} \tag{35}$$

where

$$[\bar{M}] = \begin{bmatrix} [M] & [\tilde{O}_{tt}] & [\tilde{O}_{tr}] \\ [\tilde{O}_{tt}] & [I_{tt}] & [\tilde{O}_{tr}] \\ [\tilde{O}_{rt}] & [\tilde{O}_{rt}] & [I_{rr}] \end{bmatrix}, \quad [\bar{C}] = \begin{bmatrix} [C^1_{tt}] & [\tilde{O}_{tt}] & [\tilde{O}_{tr}] \\ [\tilde{O}_{tt}] & [C^{z2}_{tt}] & [\tilde{O}_{tr}] \\ [C^3_{rt}] & [\tilde{O}_{rt}] & [C^{z3}_{rr}] \end{bmatrix}$$
$$[\bar{K}] = \begin{bmatrix} [K^1_{tt}] & [K^{z1}_{tt}] & [K^{z1}_{tr}] \\ [K^2_{tt}] & [K^{z2}_{tt}] & [\tilde{O}_{tr}] \\ [K^3_{rt}] & [K^{z3}_{rt}] & [K^{z3}_{rr}] \end{bmatrix}$$
$$\{\bar{F}\} = [(\{F^1_T\} + \{F_m\})^T \quad \{\tilde{O}_t\}^T \quad \{F^3_T\}^T]^T$$
$$\{X(t)\} = [\{X_t(t)\}^T \quad \{z_t(t)\}^T \quad \{z_r(t)\}^T]^T$$
$$[C^1_{tt}] = [C_{tt}] - [K^c_{tr}][K^c_{rr}]^{-1}[C_{rt}], \quad [K^1_{tt}] = [K^c_{tt}] - [K^c_{tr}][K^c_{rr}]^{-1}[K^c_{rt}]$$
$$[K^{z1}_{tt}] = [K^d_{tt}] - [K^c_{tr}][K^c_{rr}]^{-1}[K^d_{rt}], \quad [K^{z1}_{tr}] = [K^d_{tr}] - [K^c_{tr}][K^c_{rr}]^{-1}[K^d_{rr}]$$
$$\{F^1_T\} = \{F_{Tt}\} - [K^c_{tr}][K^c_{rr}]^{-1}\{F_{Tr}\}, \qquad [C^{z2}_{tt}] = [I_{tt}](2\hat{\omega}\,\hat{\xi})$$
$$[K^2_{tt}] = -[I_{tt}]\hat{\omega}^2, \qquad [K^{z2}_{tt}] = [I_{tt}]\hat{\omega}^2, \qquad [C^3_{rt}] = \hat{\omega}^2[K^c_{rr}]^{-1}[C_{rt}]$$
$$[C^{z3}_{rr}] = [I_{rr}](2\hat{\omega}\,\hat{\xi}), \qquad [K^3_{rt}] = \hat{\omega}^2[K^c_{rr}]^{-1}[K^c_{rt}]$$
$$[K^{z3}_{rt}] = \hat{\omega}^2[K^c_{rr}]^{-1}[K^d_{rt}], \qquad [K^{z3}_{rr}] = [I_{rr}]\hat{\omega}^2 + \hat{\omega}^2[K^c_{rr}]^{-1}[K^d_{rr}]$$
$$\{F^3_T\} = \hat{\omega}^2[K^c_{rr}]^{-1}\{F_{Tr}\} \tag{36}$$

wherein $[\tilde{O}_{tt}]$, $[\tilde{O}_{tr}]$, $[\tilde{O}_{rt}]$, $\{\tilde{O}_t\}$, and $\{\tilde{O}_r\}$ are the null matrices and vectors with the same order of $[K_{tt}]$, $[K_{tr}]$, $[K_{rt}]$, $\{z_t(t)\}$, and $\{z_r(t)\}$, respectively.

III. Numerical Results and Discussions

To assess the performance of the vertically reinforced 1-3 piezoelectric composite material as the constraining layer of the ACLD treatment for controlling the nonlinear vibrations of the FG plates under a thermal environment, the numerical results are evaluated considering a square FG substrate plate integrated with a square patch of the ACLD treatment (Fig. 1). A regular 8 by 8 mesh of eight-noded quadrilateral isoparametric elements is chosen after convergence. The linear part of the bending stiffness matrix is integrated by full integration (3×3 Gauss rule), and the nonlinear counterpart of the bending stiffness matrix and the shear stiffness matrix are integrated by reduced integration (2×2 Gauss rule) [31].

The Newmark-beta method is adopted as the numerical integration scheme, and at each time step, the direct iteration method is employed to solve the equations [35]. The value of the time step used for the integration is selected as 50 μs. The aspect ratio $s = a/h$ of the square substrate FG plate composed of zirconia and aluminum alloy is considered as 100, with the thickness of the plates being 4 mm. The thickness of the viscoelastic material layer and the piezoelectric composite material layer of the ACLD patch are considered as 50 and 250 μm, respectively.

Unless otherwise mentioned, the fiber orientation angle ψ in the piezoelectric composite constraining layer is 0 deg, the applied uniformly distributed step load acts vertically upward, and the metal-rich surface of the FG substrate plate is at the ambient temperature of 300 K. The control voltage across the thickness of the piezoelectric composite constraining layer of the ACLD patch is negatively proportional to the velocity of the midpoint ($a/2$, $b/2$, and $h/2$) of the substrate plate. Young's modulus E, the coefficient of thermal expansion α, and the thermal conductivity κ of the constituent materials of the FG plate can be expressed as the function of temperature within the temperature range of 300 K–800 K as follows [36].

Aluminum alloy:

$$E(T) = (74 + 23\times10^{-3}T - 11\times10^{-5}T^2 + 51\times10^{-9}T^3)\ \text{GPa}$$
$$\alpha(T) = (1.6\times10^{-5} + 3.45\times10^{-8}T - 3.3\times10^{-11}T^2 + 2.4\times10^{-14}T^3)\ \text{K}^{-1}, \qquad \kappa = 218\ \text{W/mK} \tag{37}$$

Zirconia:

$$E(T) = (225 - 20 \times 10^{-2}T + 90 \times 10^{-6}T^2 + 4 \times 10^{-9}T^3) \text{ GPa},$$
$$\alpha(T) = (1.48 \times 10^{-5} - 2.2 \times 10^{-8}T + 1.15 \times 10^{-11}T^2 + 4.0 \times 10^{-15}T^3) \text{ K}^{-1},$$
$$\kappa(T) = (11 \times 10^{-1} + 16 \times 10^{-5}T + 19 \times 10^{-7}T^2 - 97 \times 10^{-11}T^3) \text{ W/mK} \tag{38}$$

The temperature at any point across the thickness of the FG plate can be determined using the solution [10,15] of Eq. (12); subsequently, using Eqs. (9), (37), and (38), the effective material properties at any point in the FG plate are computed. Because the thermal conductivity of ceramic phase (zirconia) is weakly dependent on temperature variation, it is assumed as a constant having the numerical value as 1.8 W/mK. The density of the ceramic phase (zirconia) is 3000 kg/m^3 and that of the metallic phase (aluminum alloy) is 2707 kg/m^3. Poisson's ratio is assumed to be constant, having the value of 0.33 over the domain of the FG substrate plate. The material properties of the viscoelastic layer in terms of the GHM parameters are considered as [23]

$$G^{\infty} = 3.887 \times 10^4 \text{ N/m}^2, \quad \alpha_1 = 2.3263 \times 10^4$$
$$\alpha_2 = 4.1977 \times 10^1, \quad \alpha_3 = 3.5174 \times 10^1$$
$$\hat{\omega}_1 = 6.6169 \times 10^6, \quad \hat{\omega}_2 = 3.2854 \times 10^4$$
$$\hat{\omega}_3 = 4.7515 \times 10^4, \quad \hat{\xi}_1 = 3.0787, \quad \hat{\xi}_2 = 1.4288 \times 10^2$$
$$\hat{\xi}_3 = 6.1785 \times 10^2, \quad \rho = 789.5 \text{ kg/m}^3$$

The effective elastic and piezoelectric coefficients of the vertically reinforced 1-3 piezoelectric composite material are as follows [26]:

$$C_{11} = 9.293 \text{ GPa}, \quad C_{12} = 6.182 \text{ GPa}, \quad C_{13} = 6.054 \text{ GPa}$$
$$C_{33} = 35.44 \text{ GPa}, \quad C_{23} = C_{13}, \quad C_{44} = 1.58 \text{ GPa}$$
$$C_{66} = 1.54 \text{ GPa}, \quad C_{55} = C_{44}, \quad e_{31} = -0.1902 \text{ C/m}^2$$
$$e_{32} = e_{31}, \quad e_{33} = 18.4107 \text{ C/m}^2, \quad e_{24} = 0.004 \text{ C/m}^2$$
$$e_{15} = e_{24}, \quad \rho = 3000 \text{ kg/m}^3$$

The following simply supported boundary conditions are used to evaluate the numerical results:

$$v_0 = w_0 = \theta_y = 0 \quad \text{at } x = 0, a \quad \text{and}$$
$$u_0 = w_0 = \theta_x = 0 \quad \text{at } y = 0, b$$

So far, no literature is suitably available for comparing the results for the present problem being studied in this paper. Hence, to verify the implementation of the GHM method, the linear dynamic responses of a simply supported FG substrate plate are computed in the frequency domain using both the GHM method and the conventional complex-modulus approach when the patches are passive and the overall plate is in the stress-free temperature environment ($T_c = T_m = 300$ K). Note that in the finite element formulation, when $[R_{ni}]$ ($i = 1, 2, 5, 6$) are considered as null matrices, the governing equations of motion and hence Eq. (35) become linear, describing the linear behavior of the overall FG plate. In the GHM method, the frequency-response function can be computed from the following equation:

$$\{X\} = ([\bar{K}] + i\omega[\bar{C}] - \omega^2[\bar{M}])^{-1}\{\bar{F}\} \tag{39}$$

and, in the complex-modulus approach, the same can be obtained from the following equation:

$$\{X_t\} = ([K(i\omega)] - \omega^2[M])^{-1}\{F_m\} \tag{40}$$

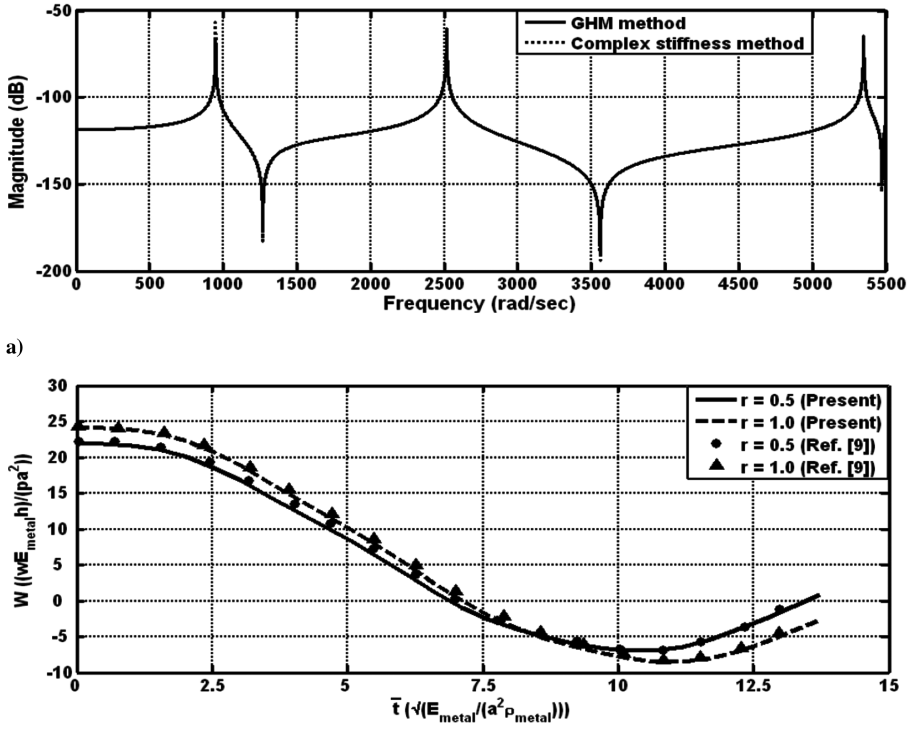

Fig. 3 Verification of the finite element model: a) the implementation of the GHM method ($a/h = 100$, $a = b$, $r = 1.0$, and $\lambda = 1$) and b) the numerical integration scheme.

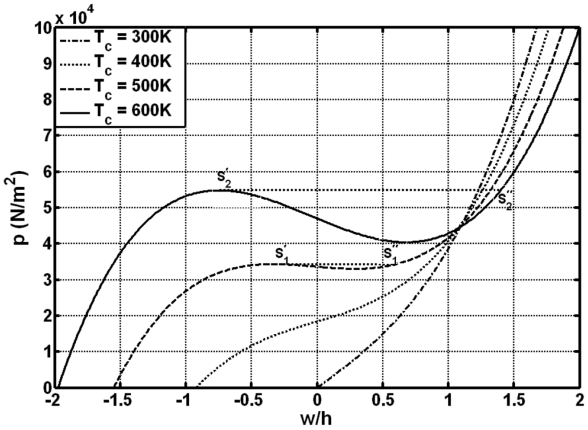

Fig. 4 Variation of center deflection of the simply supported FG substrate plate ($r = 1.0$, $\lambda = 1$, and $T_m = 300$ K) with the applied uniform pressure load.

where

$$[K(i\omega)] = ([K_{tt}] + [K^v_{tt}]G(i\omega)) - ([K_{tr}] + [K^v_{tr}]G(i\omega))([K_{rr}] + [K^v_{rr}]G(i\omega))^{-1}([K_{rt}] + [K^v_{rt}]G(i\omega)) \quad (41)$$

where $G(i\omega)$ is the complex shear modulus of the constrained viscoelastic layer. Considering a point transverse load $1e^{-i\varpi t}N$ at the point $a/4$, $b/4$, and $h/2$, with ω being the driving frequency, the frequency response for the deflection at the point $a/4$, $b/4$, and $h/2$ of the overall plate computed by the two approaches are shown in Fig. 3a. It may be observed that the frequency response by the GHM method with a single-term GHM expression ($\alpha_1 = 2.3263 \times 10^4$, $\hat{\omega}_1 = 6.6169 \times 10^6$, and $\hat{\xi}_1 = 3.0787$) is in excellent agreement with that obtained by the complex-modulus approach. For further verification of the present finite element model and the numerical integration scheme implemented to compute the nonlinear transient responses, a nonlinear transient vibration analysis is carried out in the presence of a temperature gradient through the thickness of the FG substrate plate integrated with the passive ($k_d = 0$) and negligibly thin [$(h_p + h_v) \approx 0$] ACLD patch. The transient responses at the center of this FG substrate plate are computed and compared with those of an identical FG plate without being integrated with the ACLD patch, as shown in Fig. 3b. The material properties, boundary conditions, and mechanical and thermal loading considered by Reddy [9] are used for computing the results plotted in Fig. 3b. Excellent matching of the results can be observed from this figure, verifying the present finite element model as well as the numerical integration scheme.

Because the applied mechanical load is the only disturbance to the host FG plate to cause its oscillation, the magnitude of this mechanical disturbance is to be chosen properly such that the host plate undergoes nonlinear oscillations. Such a value of the applied mechanical load can be predicted from the plots for the variation of the center deflection of the host FG substrates with the applied static mechanical load in the absence and presence of a thermal environment, as shown in Fig. 4. Thus, in the absence of a temperature gradient ($T_c = T_m = 300$ K), based on the plot illustrated in Fig. 4, the nonlinear transient responses of the simply supported thin FG substrate plates are computed considering the intensity of the uniformly distributed mechanical load as 20 kN/m^2 or more. In the presence of the temperature gradient ($T_c > 300$ K and $T_m = 300$ K), if this thin simply supported FG substrate plate with a heated ceramic-rich bottom surface is subjected to the upward mechanical load, then the FG plate may exhibit snap-through response [from S'_1 to S''_1 for $T_c = 500$ K and from S'_2 to S''_2 for $T_c = 600$ K (Fig. 4)].

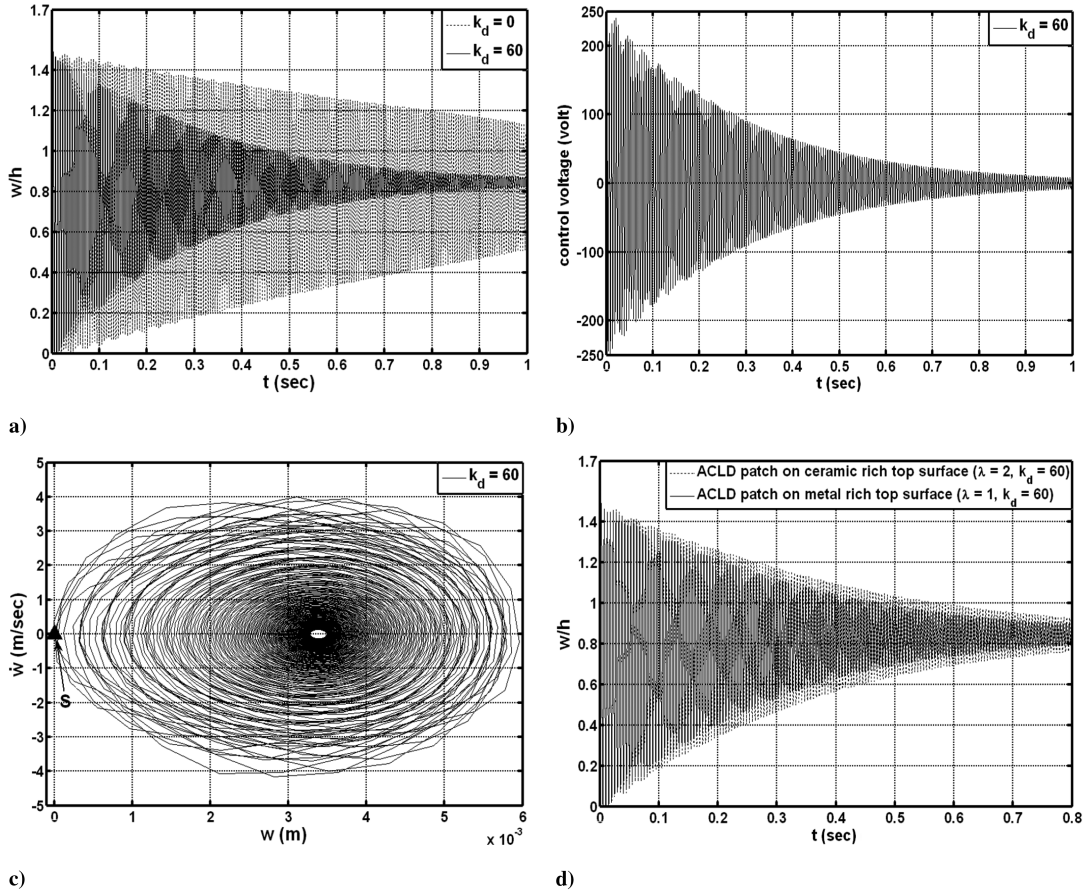

Fig. 5 Nonlinear transient responses of the overall FG plate ($T_m = T_c = 300$ K and $p = 30$ kN/m^2): a) the center deflection ($r = 1.0$ and $\lambda = 1$), b) the control voltage, c) the phase plot, and d) comparison of the responses when the patch is attached to the ceramic-rich or metal-rich surface of the host FG plate.

Hence, to avoid such instability, the value of the intensity of the applied uniformly distributed step load is considered as 20 kN/m^2 for computing the nonlinear flexural transient vibration responses of this simply supported thin FG plate.

To investigate the performance of the vertically reinforced 1-3 piezoelectric composite as the constraining layer of the ACLD treatment, the nonlinear transient responses at the midpoint of a simply supported overall FG plate under a stress-free thermal environment ($T_c = T_m = 300$ K) are illustrated in Fig. 5a. As displayed in this figure, the active ($k_d \neq 0$) piezoelectric composite constraining layer significantly increases the performance of the ACLD patch over the conventional passive ($k_d = 0$) damping. This suggests the potential use of the vertically reinforced 1-3 piezoelectric material as the constraining layer of the ACLD treatment for controlling the nonlinear vibrations of the FG plates. The control voltage presented in Fig. 5b corresponding to the gain used for the transient response shown in Fig. 5a is quite low. The phase plot shown in Fig. 5c indicates the stability of the overall plate. Figure 5d illustrates the nonlinear transient responses at the midpoint of the FG substrate plate when the patch of the ACLD treatment is attached to either the ceramic-rich or metal-rich top surfaces of the substrate plate. As displayed in this figure, the performance of the patch for controlling the nonlinear vibrations when attached to the softest surface (metal-rich) of the plate is better than that when bonded to stiffest surface (ceramic-rich) of the plate.

It is obvious that if the piezoelectric stress–strain coefficient e_{33} is considered to be zero, then the effect of the induced transverse normal stress in the active piezoelectric composite constraining layer will be absent in the computed nonlinear transient response. Hence, the contribution of this induced transverse normal stress for improving the damping characteristics of the host FG plate may be evaluated from the nonlinear transient responses when the numerical value of the piezoelectric stress–strain coefficient e_{33} is considered as zero or nonzero.

Figure 6a illustrates such transient responses for transverse displacement at the center of the overall FG plate with (e_{33}= 18.4107 N/m^2) and without ($e_{33} = 0$) considering the induced transverse normal stress in the active piezoelectric composite constraining layer of the ACLD patch. It may be observed from this figure that the induced transverse normal stress in the active piezoelectric composite constraining layer of the ACLD patch contributes significantly larger than the induced in-plane stresses in

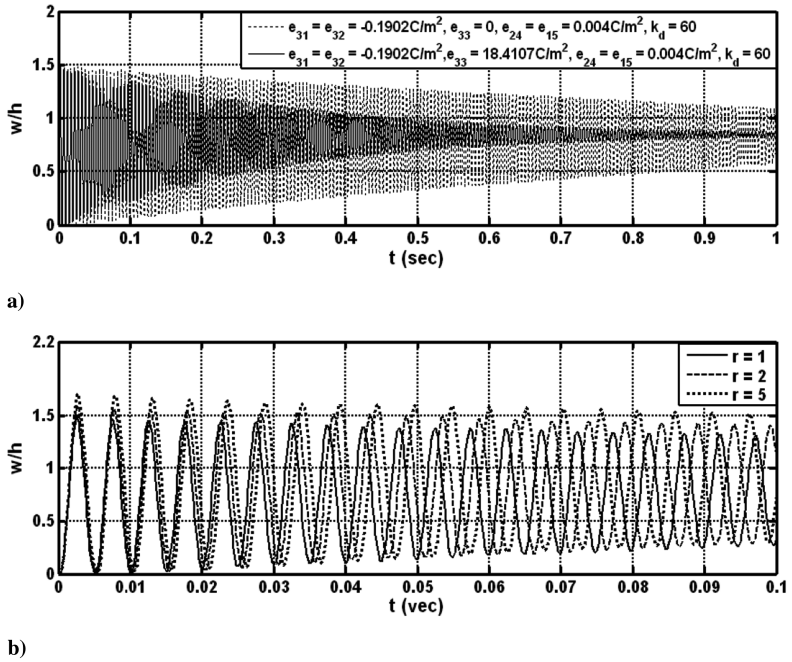

Fig. 6 Nonlinear transient responses at the center of the FG plates integrated with a patch of ACLD treatment: a) $r = 1.0$, $\lambda = 1$, $T_c = T_m = 300$ K, $p = 30$ kN/m^2, b) $\lambda = 1$, $T_c = T_m = 300$ K $p = 30$ kN/m^2, and $V_{\max} = 300$ V.

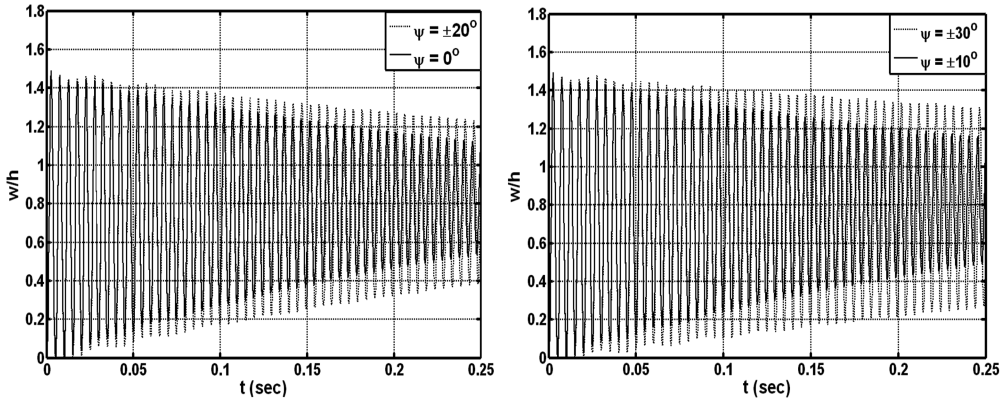

Fig. 7 Effect of piezoelectric fiber orientation angle ψ in the x–z plane of the piezoelectric composite constraining layer on the center deflection of the FG plate ($\lambda = 1$, $T_c = T_m = 300$ K, , $p = 30$ kN/m^2).

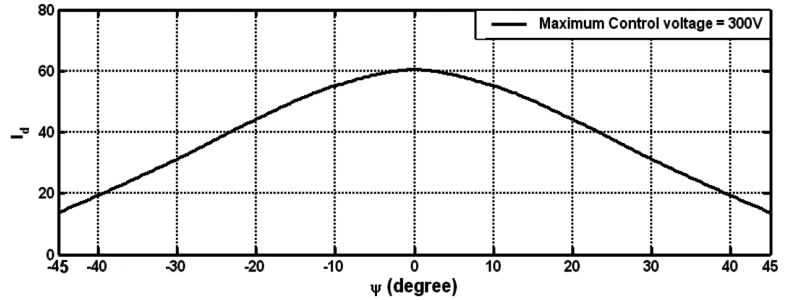

a)

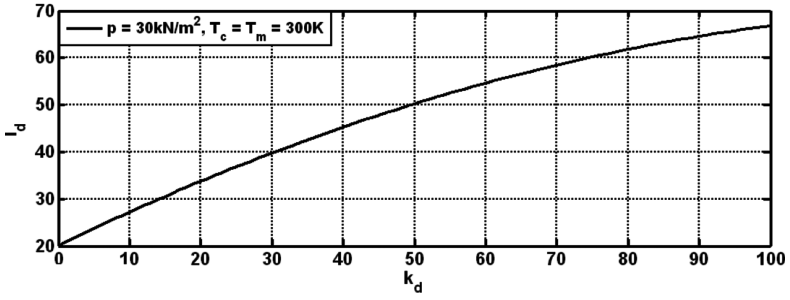

b)

Fig. 8 Effects of variations of a) piezoelectric fiber orientation angle and b) control gain on the performance of the ACLD patch attached on the top surface of the FG plate ($\lambda = 1$).

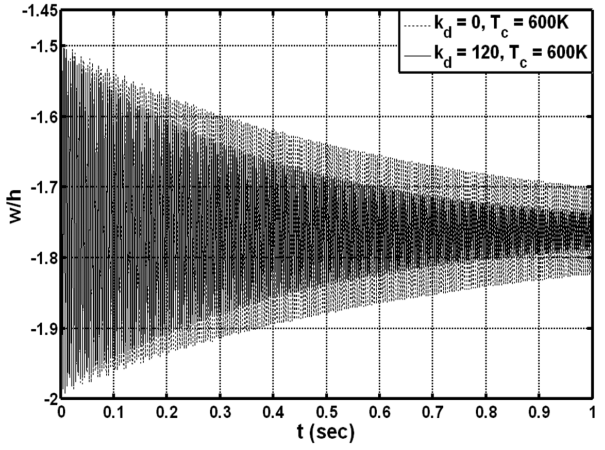

a)

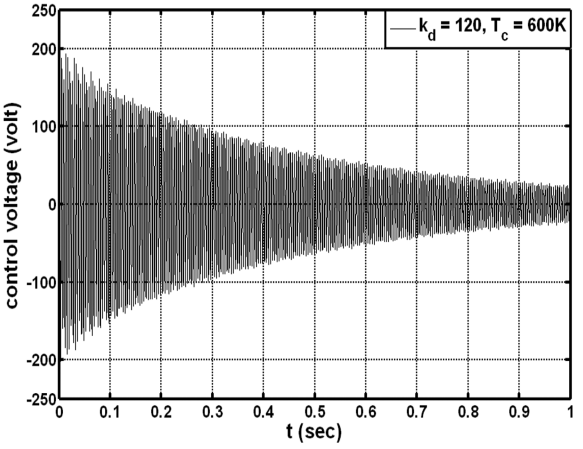

b)

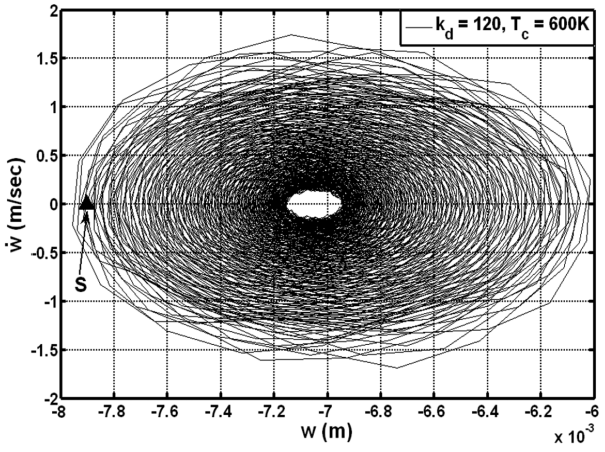

c)

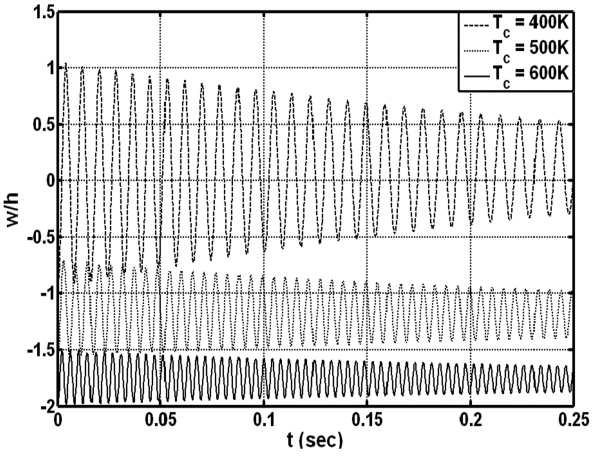

d)

Fig. 9 Nonlinear transient responses of the overall FG plate under a thermal environment ($r = 1.0$, $\lambda = 1$, $T_m = 300$ K, and $p = 20$ kN/m^2): a) the center deflection, b) the control voltage, c) the phase plot, and d) responses for different values of T_c ($V_{\max} = 300$ V).

the active piezoelectric composite constraining layer for causing active damping of the host FG plate.

The nonlinear transient responses at the center of the overall FG plates with different volume fraction index r are shown in Fig. 6b, and the maximum value of the control voltages ($V_{\max}$) for all cases is 300 V. Because a decrease in the value of the volume fraction index r causes an increase in the amount of the ceramic phase, the resulting FG substrate plate becomes stiffer. Thus, as the value of r decreases, the time period and the deflections of the plate are reduced (Fig. 6b). An important aspect of this study is to investigate the effect of variation of piezoelectric fiber orientation angle in the obliquely reinforced 1-3 piezoelectric composite constraining layer of the ACLD patch on its control authority.

For a particular value of maximum control voltage ($V_{\max}=$ 300 V), Figs. 7a and 7b illustrate the nonlinear transient responses at the center of the overall plate for different values of piezoelectric fiber orientation angle ψ, and the piezoelectric fibers are coplanar with the vertical x–z plane. It may be observed from these figures that the performance of the ACLD patch decreases as the piezoelectric fiber orientation angle in the piezoelectric composite constraining layer increases either in the clockwise (negative) or in the anti-clockwise (positive) sense from the vertical z axis. The performance of the ACLD patch does not depend on the sign of the piezoelectric fiber orientation angle. To quantify the performance of the ACLD patch for controlling the geometrically nonlinear vibrations of the FG substrate plates, a performance index is defined as follows:

$$I_d = \frac{A_{t=0} - A_{t=0.25s}}{A_{t=0}} \times 100 \tag{42}$$

where I_d measures the percentage diminution of amplitude of nonlinear transient vibrations of the overall plate after 0.25 s. For a particular value of maximum control voltage ($V_{\max} = 300$ V), the variation of this index with the variation of the piezoelectric fiber orientation angle from −45 to 45 deg has been illustrated in Fig. 8a. It may be observed from this figure that the performance of the ACLD patch is maximum when the piezoelectric fiber orientation angle in the piezoelectric composite constraining layer is 0 deg. As expected, the variation of the control gain affects the performance of the patch in a nonlinear fashion, as shown in Fig. 8b.

Similar to the results in the absence of a thermal environment (Fig. 5a), the vertically reinforced 1-3 piezoelectric composite constraining layer is also capable of increasing the active damping characteristics of the overall plate over the passive damping in the presence of the temperature gradient through the thickness of the host FG plate, as shown in Fig. 9a. Because the mechanical load and the temperature field across the thickness of the FG substrate plate with a heated ceramic-rich bottom surface cause upward and downward deflections of the overall FG plate, respectively, the vibrations of the overall plate occur about an equilibrium position that is displaced in the negative (downward) direction, as shown in Fig. 9a. The control voltage illustrated corresponding to the gain used for the transient response shown in Fig. 9a is quite low and has been plotted in Fig. 9b. The phase plot shown in Fig. 9c indicates the stability of the overall FG plate under the thermal environment. Figure 9d illustrates the nonlinear transient responses at the center of the overall FG plate for different values of the temperature of the ceramic-rich bottom surface of the FG substrate plate, and the metal-rich top surface of the same is exposed to the room temperature. The maximum value of the control voltages ($V_{\max}$) for the responses in Fig. 9d is 300 V. As displayed in this figure, when the temperatures of the ceramic-rich bottom surface of the host FG plate are 400, 500, and 600 K, the amplitudes of vibrations are reduced by 57.74, 50.1, and 49.02%, respectively, after 0.25 s. Thus, the performance of the ACLD patch decreases

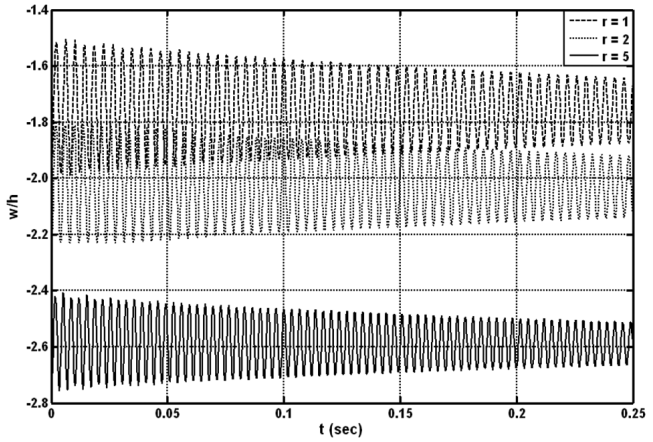

Fig. 10 Controlled nonlinear transient responses at the center of the simply supported overall FG plates with different values of r ($\lambda = 1$, $T_m = 300$ K, $T_c = 600$ K, $p = 20$ kN/m^2, and $V_{\max} = 300$ V).

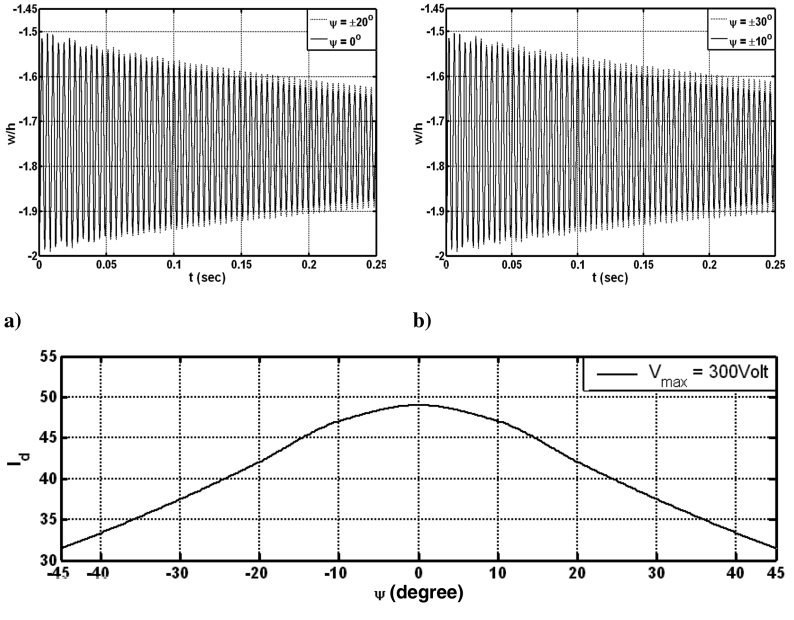

Fig. 11 Effect of piezoelectric fiber orientation angle ψ in the x–z plane of the piezoelectric composite constraining layer of the ACLD patch attached on the top surface of the FG plate under a thermal environment ($\lambda = 1$, $T_c = 600$ K, $T_m = 300$ K, $V_{\max} = 300$ V, and $p = 20$ kN/m^2).

with the rise in the temperature of the ceramic-rich bottom surface of the host FG plate.

For a particular value of the temperature of the heated ceramic-rich surface ($T_c = 600$ K) of the FG plate, Fig. 10 exhibits that as the value of the volume fraction index r increases, the initial deflection of the plate increases, and the time period and the amplitude of vibrations of the plate are reduced. The FG plate is basically an antisymmetric plate wherein the coupling of stretching and bending deformations occurs. Thus, when the plate is not subjected to the applied mechanical load, the plate undergoes initial bending deflections due to the stretching of the plate caused by applied thermal gradient. If the effective coefficient of thermal expansion of the plate increases, this initial bending will be enhanced, which is the case when the metallic constituent of the plate increases due to the increase in the value of r.

In the presence of a temperature gradient across the thickness of the host FG plate, the nonlinear transient responses at the center of the overall plate for different piezoelectric fiber orientation angles in the piezoelectric constraining layer are plotted in Figs. 11a and 11b and maintain the same value of maximum control voltages for all cases. It may be observed from these figures that the performance of the ACLD patch decreases as the piezoelectric fiber orientation angle ψ increases either in the negative (clockwise) or in the positive (anticlockwise) direction from the vertical z axis. In Fig. 11c, the variation of performance index I_d within a range of piezoelectric fiber orientation angles from -45 to 45 deg exhibits that the performance of the ACLD patch is maximum when the piezoelectric fibers are parallel to the vertical z axis ($\psi = 0$ deg).

IV. Conclusions

This paper is concerned with the investigation of the performance of the vertically and obliquely reinforced 1-3 piezoelectric composite materials for active-constrained-layer damping (ACLD) of smart functionally graded (FG) plates undergoing geometrically nonlinear transient vibrations in the thermal environment. A three-dimensional finite element model has been developed for the functionally graded plates integrated with a patch of ACLD treatment, and the constraining layer of the ACLD treatment is considered to be composed of the vertically/obliquely reinforced 1-3 piezoelectric composite.

The novelty of the finite element model is that both in-plane and transverse actuations by the constraining layer of the ACLD treatment have been used for active damping of nonlinear vibrations of the host FG plates. The temperature field is assumed to be spatially uniform over the substrate plate surfaces, and it varies across the thickness of the host FG plates. The temperature-dependent material properties of the FG substrate plates are graded in the thickness direction according to a simple power-law distribution, and Poisson's ratio of the plates is assumed to be a constant.

For the time-domain analysis, the viscoelastic constrained layer of the ACLD patch is modeled using the Golla–Hughes–McTavish method. The kinematics of deformation of the overall plate is defined based on the first-order shear deformation theory. The numerical results revealed that using the vertically reinforced 1-3 piezoelectric composite material as the constraining layer of the ACLD patch significantly improves the damping characteristics of the FG plates over the passive damping for controlling the nonlinear vibrations of the plates in the absence and presence of the temperature gradient across the thickness of the plates. The performance of the ACLD patch decreases with the increase of the temperature gradient through the thickness of the FG plate. The analysis reveals that if the volume fraction index of the FG plate increases, then the time period and the amplitudes of the controlled response decrease under a thermal environment. The analysis also reveals that the performance of the ACLD patch is more when it is attached on the softest surface of the host FG plate than when it is attached on the stiffest surface of the same. More important, it is found that the contribution of transverse actuation by the constraining layer of the ACLD patch for causing active damping of the host FG plate is significantly larger than that of in-plane actuation by the same. The best performance of the ACLD patch is attained when the piezoelectric fiber orientation angle in the active constraining layer of the patch is 0 deg with respect to the vertical z axis.

Appendix: Matrices Appearing in Eq. (7)

$$[Z_1^k] = \begin{bmatrix} 1 & 0 & 0 \\ 0 & 1 & 0 \\ 0 & 0 & 1 \\ 0 & 0 & 0 \end{bmatrix}, \quad [Z_{n1}^k] = \begin{bmatrix} 1/2 & 0 & 0 \\ 0 & 1/2 & 0 \\ 0 & 0 & 1 \\ 0 & 0 & 0 \end{bmatrix}$$

$$[Z_{n5}^k] = \begin{bmatrix} [{}_sZ_{n5}^k] & [0] & [0] \\ [0] & [{}_sZ_{n5}^k] & [0] \\ [0] & [0] & [{}_sZ_{n5}^k] \\ [0] & [0] & [0] \end{bmatrix}$$

$$[Z_3^k] = [I]_{2\times 2}, \quad [Z_2^k] = [[Z_{2i}^k]_{i=1} \;\; [Z_{2i}^k]_{i=2} \;\; [Z_{2i}^k]_{i=3}]$$

$$[Z_4^k] = [[Z_{4i}^k]_{i=1} \;\; [Z_{4i}^k]_{i=2} \;\; [Z_{4i}^k]_{i=3}]$$

$$[Z_{n2}^k] = [[Z_{n2ij}^k]_{i=1,j=2} \;\; [Z_{n2ij}^k]_{i=2,j=3} \;\; [Z_{n2ij}^k]_{i=3,j=1}]$$

$$[Z_5^k] = [Z_1^k], \quad [Z_6^k] = [Z_2^k], \quad [Z_7^k] = [Z_3^k], \quad [Z_8^k] = [Z_4^k]$$

$$[Z_{n6}^k] = [[Z_{n6ijm}^k]_{i=1,j=2,m=3} \;\; [Z_{n6ijm}^k]_{i=2,j=1,m=3} \;\; [Z_{n6ijm}^k]_{i=3,j=1,m=2}]$$

$$[R_{n1}] = \begin{bmatrix} \partial w_0/\partial x & 0 \\ 0 & \partial w_0/\partial y \\ \partial w_0/\partial y & 0 \end{bmatrix}$$

$$[R_{n2}] = \begin{bmatrix} [R_{n2i}]_{i=1} & [0] & [0] \\ [0] & [R_{n2i}]_{i=2} & [0] \\ [0] & [0] & [R_{n2i}]_{i=3} \end{bmatrix}$$

$$[R_{n5}] = \begin{bmatrix} \partial\{{}_sR_{n5}\}/\partial x & [0] & \partial\{{}_sR_{n5}\}/\partial y \\ [0] & \partial\{{}_sR_{n5}\}/\partial y & \partial\{{}_sR_{n5}\}/\partial x \end{bmatrix}^T$$

$$[R_{n6}] = \begin{bmatrix} [R_{n6i}]_{i=1} & [0] & [0] \\ [0] & [R_{n6i}]_{i=2} & [0] \\ [0] & [0] & [R_{n6i}]_{i=3} \end{bmatrix}$$

where $[I]$ is the unit matrix and the various submatrices are as follows:

$$[Z_{2i}^k] = \begin{bmatrix} z_i^k & 0 & 0 & 0 \\ 0 & z_i^k & 0 & 0 \\ 0 & 0 & z_i^k & 0 \\ 0 & 0 & 0 & \partial z_i^k/\partial z \end{bmatrix}$$

$$[Z_{4i}^k] = \begin{bmatrix} \partial z_i^k/\partial z & 0 & z_i^k & 0 \\ 0 & \partial z_i^k/\partial z & 0 & z_i^k \end{bmatrix}$$

$$[Z_{n2ij}^k] = \begin{bmatrix} [{}_s^1Z_{n2ij}^k] & [0] & [0] \\ [0] & {}_s^1[Z_{n2ij}^k] & [0] \\ [0] & [0] & {}_s^2[Z_{n2ij}^k] \\ [0] & [0] & [0] \end{bmatrix}$$

$$[Z_{n6ijm}^k] = \begin{bmatrix} [{}_sZ_{n6ijm}^k] & [0] & [0] \\ [0] & [{}_sZ_{n6ijm}^k] & [0] \\ [0] & [0] & [{}_sZ_{n6ijm}^k] \\ [0] & [0] & [0] \end{bmatrix}$$

$$ {}^{1}_{s}[Z^{k}_{n2ij}] = [\,1/2(z^{k}_{i})^{2} \quad z^{k}_{i} \quad z^{k}_{i}z^{k}_{j}\,],\ {}^{2}_{s}[Z^{k}_{n2ij}] = [\,z^{k}_{i} \quad (z^{k}_{i})^{2} \quad z^{k}_{i}z^{k}_{j}\,] $$

$$ [{}_{s}Z^{k}_{n6ijm}] = [\,(z^{k}_{i})^{2} \quad z^{k}_{i} \quad z^{k}_{i}z^{k}_{j} \quad z^{k}_{i}z^{k}_{m}\,] $$

$$ [{}_{s}Z^{k}_{n5}] = [\,1 \quad z^{k}_{1} \quad z^{k}_{2} \quad z^{k}_{3}\,] $$

$$ [R_{n2i}] = \begin{bmatrix} \partial\{{}^{1}_{s}\boldsymbol{R}_{n2i}\}/\partial x & [0] & \partial\{{}^{2}_{s}\boldsymbol{R}_{n2i}\}/\partial y \\ [0] & \partial\{{}^{1}_{s}\boldsymbol{R}_{n2i}\}/\partial y & \partial\{{}^{3}_{s}\boldsymbol{R}_{n2i}\}/\partial x \end{bmatrix}^{T} $$

$$ [R_{n6i}] = \begin{bmatrix} \partial\{{}_{s}\boldsymbol{R}_{n6i}\}/\partial x & [0] & \partial\{{}_{s}\boldsymbol{R}_{n6i}\}/\partial y \\ [0] & \partial\{{}_{s}\boldsymbol{R}_{n6i}\}/\partial y & \partial\{{}_{s}\boldsymbol{R}_{n6i}\}/\partial x \end{bmatrix}^{T} $$

$$ \{{}^{1}_{s}\boldsymbol{R}_{n2i}\}_{i=1} = [\,\theta_z \quad w_0 \quad \phi_z\,], \qquad \{{}^{2}_{s}\boldsymbol{R}_{n2i}\}_{i=1} = [\,w_0 \quad 0 \quad \phi_z\,] $$

$$ \{{}^{3}_{s}\boldsymbol{R}_{n2i}\}_{i=1} = [\,w_0 \quad \theta_z \quad \phi_z\,] $$

$$ \{{}^{1}_{s}\boldsymbol{R}_{n2i}\}_{i=2} = [\,\phi_z \quad w_0 \quad \gamma_z\,], \qquad \{{}^{2}_{s}\boldsymbol{R}_{n2i}\}_{i=2} = [\,w_0 \quad 0 \quad \gamma_z\,] $$

$$ \{{}^{3}_{s}\boldsymbol{R}_{n2i}\}_{i=2} = [\,w_0 \quad \phi_z \quad \gamma_z\,] $$

$$ \{{}^{1}_{s}\boldsymbol{R}_{n2i}\}_{i=3} = [\,\gamma_z \quad w_0 \quad \theta_z\,], \qquad \{{}^{2}_{s}\boldsymbol{R}_{n2i}\}_{i=3} = [\,w_0 \quad 0 \quad \theta_z\,] $$

$$ \{{}^{3}_{s}\boldsymbol{R}_{n2i}\}_{i=3} = [\,w_0 \quad \gamma_z \quad \theta_z\,] $$

$$ \{{}_{s}\boldsymbol{R}_{n6i}\}_{i=1} = [\,\theta_z \quad w_0 \quad \phi_z \quad \gamma_z\,] $$

$$ \{{}_{s}\boldsymbol{R}_{n6i}\}_{i=2} = [\,\phi_z \quad w_0 \quad \theta_z \quad \gamma_z\,] $$

$$ \{{}_{s}\boldsymbol{R}_{n6i}\}_{i=3} = [\,\gamma_z \quad w_0 \quad \theta_z \quad \phi_z\,] $$

$$ \{{}_{s}\boldsymbol{R}_{n5}\} = [\,w_0 \quad \theta_z \quad \phi_z \quad \gamma_z\,] $$

References

[1] Koizumi, M., "Concept of FGM," *Ceramic Transactions*, Vol. 34, 1993, pp. 3–10.

[2] Teymur, M., Chitkara, N. R., Yohngjo, K., Aboudi, J., Pindera, M. J., and Arnold, S. M., "Thermoelastic Theory for the Response of Materials Functionally Graded in Two Directions," *International Journal of Solids and Structures*, Vol. 33, No. 7, 1996, pp. 931–966.

[3] Mian, A. M., and Spencer, A. J. M., "Exact Solutions for Functionally Graded and Laminated Elastic Materials," *Journal of the Mechanics and Physics of Solids*, Vol. 46, No. 12, 1998, pp. 2283–2295. doi:10.1016/S0022-5096(98)00048-9

[4] Batra, R. C., and Vel, S. S., "Exact Solution for Thermoelastic Deformations of Functionally Graded Thick Rectangular Plates," *AIAA Journal*, Vol. 40, No. 7, 2001, pp. 1421–1433.

[5] Loy, C. T., Lam, K. Y., and Reddy, J. N., "Vibration of Functionally Graded Cylindrical Shells," *International Journal of Mechanical Sciences*, Vol. 41, No. 3, 1999, pp. 309–324.

[6] Vel, S. S., and Batra, R. C., "Three-Dimensional Analysis of Transient Thermal Stresses in Functionally Graded Plates," *International Journal of Solids and Structures*, Vol. 40, No. 25, 2003, pp. 7181–7196. doi:10.1016/S0020-7683(03)00361-5

[7] Yang, J., and Shen, H. S., "Dynamic Response of Initially Stressed Functionally Graded Rectangular Thin Plates," *Composite Structures*, Vol. 54, No. 4, 2001, pp. 497–508. doi:10.1016/S0263-8223(01)00122-2

[8] Praveen, G. N., and Reddy, J. N., "Nonlinear Transient Thermoelastic Analysis of Functionally Graded Ceramic Metal Plates," *International Journal of Solids and Structures*, Vol. 35, No. 33, 1998, pp. 4457–4476. doi:10.1016/S0020-7683(97)00253-9

[9] Reddy, J. N., "Analysis of Functionally Graded Plates," *International Journal for Numerical Methods in Engineering*, Vol. 47, Nos. 1-3, 2000, pp. 663–684. doi:10.1002/(SICI)1097-0207(20000110/30)47:1/3<663::AID-NME787>3.0.CO;2-8

[10] Woo, J., and Meguid, S. A., "Nonlinear Analysis of Functionally Graded Plates and Shallow Shells," *International Journal of Solids and Structures*, Vol. 38, Nos. 42–43, 2001, pp. 7409–7421. doi:10.1016/S0020-7683(01)00048-8

[11] Shen, H. S., "Nonlinear Bending Response of Functionally Graded Plates Subjected to Transverse Loads and in Thermal Environments," *International Journal of Mechanical Sciences*, Vol. 44, No. 3, 2002, pp. 561–584. doi:10.1016/S0020-7403(01)00103-5

[12] Bailey, T., and Hubbard, J. E., "Distributed Piezoelectric Polymer Active Vibration Control of a Cantilever Beam," *Journal of Guidance, Control, and Dynamics*, Vol. 8, No. 5, 1985, pp. 605–611. doi:10.2514/3.20029

[13] Miller, S. E., and Hubbard, J. E., "Observability of a Bernoulli-Euler Beam Using PVF_2 as a Distributed Sensor," MIT Draper Lab., Cambridge, MA, July 1987.

[14] Liew, K. M., He, X. Q., Ng, T. Y., and Kitipornchai, S., "Finite Element Piezo-Thermo-Elasticity Analysis and Active Control of FGM Plates with Integrated Piezoelectric Sensors and Actuators," *Computational Mechanics*, Vol. 31, Nos. 3–4, 2003, pp. 350–358.

[15] Yang, J., Kitipornchai, S., and Liew, K. M., "Non-Linear Analysis of Thermo-Electromechanical Behavior of Shear Deformable FGM Plates with Piezoelectric Actuators," *International Journal for Numerical Methods in Engineering*, Vol. 59, No. 12, 2004, pp. 1605–1632. doi:10.1002/nme.932

[16] Huang, X.-L., and Shen, H.-S., "Vibration and Dynamic Response of Functionally Graded Plates with Piezoelectric Actuators in Thermal Environments," *Journal of Sound and Vibration*, Vol. 289, Nos. 1–2, 2006, pp. 25–53. doi:10.1016/j.jsv.2005.01.033

[17] Baz, A., and Ro, J., "Optimum Design and Control of Active Constrained Layer Damping," *Journal of Mechanical Design*, Vol. 117, No. 1, 1995, pp. 135–144. doi:10.1115/1.2836447

[18] Baz, A., and Ro, J., "Vibration Control of Plates with Active Constrained Layer Damping," *Smart Materials and Structures*, Vol. 5, No. 3, 1995, pp. 272–280.

[19] Ray, M. C., and Baz, A., "Optimization of Energy Dissipation of Active Constrained Layer Damping Treatment of Plates," *Journal of Sound and Vibration*, Vol. 208, No. 3, 1997, pp. 391–406.

[20] Lam, M. J., Inman, D. J., and Saunders, W. R., "Hybrid Damping Models Using the Golla–Hughes–McTavish Method with Internally Balanced Model Reduction and Output Feedback," *Smart Materials and Structures*, Vol. 9, No. 3, 2000, pp. 362–371. doi:10.1088/0964-1726/9/3/318

[21] Ray, M. C., Oh, J., and Baz, A., "Active Constrained Layer Damping of Thin Cylindrical Panels," *Journal of Sound and Vibration*, Vol. 240, No. 5, 2001, pp. 921–935.

[22] Lim, Y.-H., Varadan, V. V., and Varadan, V. K., "Closed-Loop Finite Element Modeling of Active Constrained Layer Damping in the Time Domain Analysis," *Smart Materials and Structures*, Vol. 11, No. 1, 2002, pp. 89–97. doi:10.1088/0964-1726/11/1/310

[23] Shi, Y., Hua, H., and Sol, H., "The Finite Element Analysis and Experimental Study of Beams with Active Constrained Layer Damping Treatments," *Journal of Sound and Vibration*, Vol. 278, Nos. 1–2, 2004, pp. 343–363. doi:10.1016/j.jsv.2003.10.009

[24] Smith, W. A., and Auld, B. A., "Modeling 1-3 Composite Piezoelectrics: Thickness Mode Oscillations," *IEEE Transactions on Ultrasonics, Ferroelectrics and Frequency Control*, Vol. 38, No. 1, 1991, pp. 40–47. doi:10.1109/58.67833

[25] Ray, M. C., and Pradhan, A. K., "The Performance of Vertically Reinforced 1-3 Piezoelectric Composites in Active Damping of Smart Structures," *Smart Materials and Structures*, Vol. 15, No. 1, 2006, pp. 631–641.

[26] Ray, M. C., and Pradhan, A. K., "On the Use of Vertically Reinforced 1-3 Piezoelectric Composites for Hybrid Damping of Laminated Composite Plates," *Mechanics of Advanced Materials and Structures*, Vol. 14, No. 4, 2007, pp. 245–261.

[27] Panda, S., and Ray, M. C., "Geometrically Nonlinear Analysis of Smart Functionally Graded Plates Integrated with a Layer of Vertically Reinforced 1-3 Piezoelectric Composite," *Acta Mechanica*, Vol. 198, Nos. 3–4, 2008.doi:10.1007/s00707-007-0529-6

[28] Panda, S., and Ray, M. C., "Finite Element Analysis For Geometrically Nonlinear Deformations of Smart Functionally Graded Plates Using Vertically Reinforced 1-3 Piezoelectric Composite," *International Journal of Mechanics and Materials in Design*, Vol. 4, No. 3, 2008.doi:10.1007/s10999-008-9054-6

[29] Golla, D. F., and Hughes, P. C., "Dynamics of Viscoelastic Structures: A Time-Domain, Finite Element Formulation," *Journal of Applied Mechanics*, Vol. 52, No. 6, 1985, pp. 897–906.

[30] McTavish, D. J., and Hughes, P. C., "Modeling of Linear Viscoelastic Space Structures," *Journal of Vibration and Acoustics*, Vol. 115, No. 1, 1993, pp. 103–133. doi:10.1115/1.2930302

[31] Reddy, J. N., *An Introduction to Nonlinear Finite Element Analysis*, Oxford Univ. Press, New York, 2004.
[32] Christensen, R. M., *Theory of Viscoelasticity: An Introduction*, 2nd ed., Academic Press, New York, 1982.
[33] Tiersten, H. F., "Linear Piezoelectric Plate Vibrations," Plenum, New York, 1969.
[34] Kim, T.-W., and Kim, J.-H., "Nonlinear Vibration of Viscoelastic Laminated Composite Plates," *International Journal of Solids and Structures*, Vol. 39, No. 10, 2002, pp. 2857–2870. doi:10.1016/S0020-7683(01)00272-4
[35] Cook, R. D., Malkus, D. S., Plesha, M. E., and Witt, R. J., "Concepts and Applications of Finite Element Analysis," Wiley, Hoboken, NJ, 2002.
[36] Noda, N., "Thermal Stresses in Functionally Graded Materials," *Journal of Thermal Stresses*, Vol. 22, No. 4-5, 1999, pp. 477–512. doi:10.1080/014957399280841

F. Pai
Associate Editor